

Experimental Evaluation of the Static Strength and Ductility of Large Diameter Shear Studs in Composite Bridge Construction

by

Jason Veclotch

A thesis submitted to the Graduate Faculty of
Auburn University
in partial fulfillment of the
requirements for the Degree of
Master of Science

Auburn, Alabama
May 5, 2013

Approved by

Hassan Abbas, Chair, Assistant Professor of Structural Engineering
G. Ed Ramey, Professor Emeritus of Structural Engineering
Robert Barnes, James J. Mallett Associate Professor of Structural Engineering
J. Michael Stallings, Head of the Department of Civil Engineering

Abstract

A number of bridges in the United States consist of steel girders with concrete decks attached via shear studs which will require replacement in the future. With a growing interest in rapid deck replacement for bridges as the nation's infrastructure ages and traffic congestion concerns increase, one possible means to accelerate the replacement process is the use of large diameter, 1.25" shear studs, which would reduce the total number of shear connectors needed. The use of these studs is not addressed in the current AASHTO LRFD Bridge Specifications. An experimental procedure was developed to comparatively evaluate the strength and ductility of 1.25" diameter shear studs in two configurations to conventional stud sizes, in this case 7/8" diameter. Flexural strength testing was conducted on four beams, 34 feet in length, with W21x44 steel sections acting compositely with 7" thick, 3 feet wide reinforced concrete decks. The results indicate that a reduced number of these large diameter studs do provide adequate strength and ductility for use in composite bridge construction. The research indicates that structures with 1.25" large diameter shear studs may be safely designed using current strength provisions of the AASHTO LRFD Bridge Design Specifications.

Acknowledgements

I wish to thank my advisor, Dr. Abbas, and all my committee members whose advice and extensive technical expertise was invaluable in successfully completing this research and expanding my own knowledge of the related subject matter.

I would also like to give special thanks to undergraduate research assistant Carrie Field, who spent many hours in the lab during experimental setup and testing performing high quality work and bringing in fresh perspectives, helping to overcome the numerous challenges encountered during testing.

Additionally I would like to mention Adam Wilkinson, Billy Wilson, Patrick Kimmons, Travis Bugg, Dave Mante, Daniel Mundie, K.C. Lee, and everyone else who made contributions to various aspects of this research.

I am also thankful for the personal support given to me by my parents and Jessica Ridley as I worked to finish my research efforts and thesis.

Table of Contents

Abstract.....	ii
Acknowledgements	iii
List of Tables	vii
List of Figures	viii
List of Symbols	xi
Chapter 1: Introduction	1
Section 1.1 Overview	1
Section 1.2 Motivation	3
Section 1.3 Objectives	5
Section 1.4 Research Tasks	5
Section 1.5 Scope and Approach	6
Section 1.6 Thesis Organization	6
Chapter 2: Background and Literature Review	8
Section 2.1 Overview	8
Section 2.2 Review of Current Design Provisions	8
Section 2.3 Previous Research	12
Chapter 3: Test Program and Protocol	18
Section 3.1 Overview	18
Section 3.2 Specimen Design and Configuration	18

Section 3.3 Material Properties	22
Section 3.4 Specimen Fabrication	26
Section 3.5 Test Setup	31
Section 3.6 Instrumentation	35
Section 3.7 Loading Protocol	41
Chapter 4: Results and Data Analysis	44
Section 4.1 Overview	44
Section 4.2 Numerical Sign Conventions	44
Section 4.3 Partial Composite Action Analysis and Results	46
Section 4.4 Qualitative Observations and Analysis	51
Section 4.5 Numerical Results and Analysis	64
Chapter 5: Conclusions and Recommendations	85
Section 5.1 Overview	85
Section 5.2 Conclusions	85
Section 5.3 Design Code Recommendations	87
Section 5.4 Future Research Recommendations	87
References	89
Appendix 1: Mill Reports	91
Section A1.1 W21x44 Mill Test Report.....	91
Section A1.2 7/8" Diameter Shear Stud Mill Test Report.....	92
Section A1.3 1.25" Diameter Shear Stud Mill Test Report	96
Section A1.4 Rebar Mill Test Report.....	98
Appendix 2: Additional Concrete Data and Reports	99

Section A2.1 Concrete Batch 1 Report	99
Section A2.2 Concrete Batch 2 Report	100
Section A2.3 Complete Batch 1 Cylinder Test Data	101
Section A2.4 Complete Batch 2 Cylinder Test Data	102

List of Tables

Table 3.3-1: Steel Component Material Properties	22
Table 3.3-2: Concrete Cylinder Test Compression Strengths	25
Table 3.3-3: Steel Component Measured Dimensions	26
Table 3.3-4: Concrete Deck Measured Dimensions	26
Table 3.3-5: Shear Stud Measured Diameters	26
Table 4.3-1: Specimen Configurations and Degree of Composite Action	49
Table 4.3-2: Theoretical and Experimental Moment Capacities	49
Table 4.5-1: Midspan Deflections with 70K at Midspan (Elastic)	66
Table 4.5-2: Midspan Deflections Under Peak Applied Moment	66
Table 4.5-3: Cumulative Slip Values at Peak Applied Moment.....	70
Table A2.3-1: Complete Cylinder Test Data for Concrete Batch 1	100
Table A2.4-1: Complete Cylinder Test Data for Concrete Batch 2	101

List of Figures

Figure 1.1-1: A pair of headed shear stud connectors welded to a steel flange	2
Figure 3.2-1: Transverse cross section view of specimen configurations	20
Figure 3.2-2: Longitudinal cross section view of specimen configurations	21
Figure 3.4-1: A stud welding gun with modified cradle welds a large diameter shear stud to the top flange of a test specimen	28
Figure 3.4-2: A typical high quality weld of a large diameter stud on a test specimen	28
Figure 3.4-3: Fully assembled concrete formwork	29
Figure 3.4-4: Casting of concrete deck from overhead hopper	31
Figure 3.5-1: Load application system under actuator	32
Figure 3.5-2: Roller support assembly and stability bracing	33
Figure 3.5-3: Pin support assembly.....	34
Figure 3.5-4: Support strap safety system	35
Figure 3.6-1: Draw wire vertical displacement sensor	36
Figure 3.6-2: Draw wire, laser, and piston type (position) displacement sensor	37
layout	
Figure 3.6-3: Piston type sensor with mounting block and contact block	38
Figure 3.6-4: Laser displacement sensor and target	39
Figure 3.6-5: Typical strain gage cross section patterns	40
Figure 3.7-1: Loading configuration and moment due to applied loads diagram.....	42
Figure 4.4-1: Beam specimen under load at midspan	54

Figure 4.4-2: Deflection of beam specimen under load at midspan and quarterspan	55
Figure 4.4-3: Striations visible in web of steel section at midspan	56
Figure 4.4-4: Flakes of surface material from the steel	57
section accumulating under the specimen	
Figure 4.4-5: Tension cracks forming in the bottom side of the concrete deck at midspan	58
Figure 4.4-6: Crushing at top of deck and cracking at bottom of the deck for Specimen 1	59
Figure 4.4-7: Deflected shape of Specimen 3 after failure	60
Figure 4.4-8: Concrete deck failure of Specimen 2	61
Figure 4.4-9: Concrete deck failure in Specimen 3	62
Figure 4.4-10: Cracking in bottom of deck for Specimen 4 after failure	63
Figure 4.4-11: Crushing of concrete deck for Specimen 4 after failure	63
Figure 4.5-1: Plot of Midspan Moment vs. Midspan Vertical Deflection	65
Figure 4.5-2: Plot of the Ratio of Applied Midspan Moment to Theoretical	67
Moment Capacity vs. the Vertical Deflection at Midspan	
Figure 4.5-3: Plot of Midspan Moment vs. Cumulative Slab Slip	69
Figure 4.5-4: Plot of the Ratio of Moment to Theoretical	70
Moment Capacity vs. Cumulative Slab Slip	
Figure 4.5-5: Plot of Measured Slip vs Distance Along the Beam with 70 K at	72
Midspan and Elastic Behavior	
Figure 4.5-6: Plot of Measured Slip vs Distance Along the Beam at Peak Moment.....	73
Figure 4.5-7: Plot of Stud Slip vs Distance Along Beam with 70 K at	76
Midspan and Elastic Behavior for Specimens 1 and 2	
Figure 4.5-8: Plot of Stud Slip vs Distance Along Beam with 70 K at	77
Midspan and Elastic Behavior for Specimens 3 and 4	
Figure 4.5-9: Plot of Stud Slip vs Distance Along Beam at Peak Applied	78
Moment for Specimens 1 and 2	

Figure 4.5-10: Plot of Stud Slip vs Distance Along Beam at Peak Applied Moment for Specimens 3 and 479

Figure 4.5-11: 3/8th span strain profile with 70 K at midspan81

Figure 4.5-12: 3/8th span strain profile under peak applied moment at midspan83

List of Symbols

a	= the depth of the equivalent stress block in the concrete deck
A_{sc}	= shear stud cross sectional area
b_{fc}	= width of the steel top flange
b_{ft}	= width of the steel bottom flange
b_s	= effective width of the concrete deck
d_1	= The distance from the centroid of the compressive force in the concrete deck to the top of the steel section
d_2	= The distance from the centroid of the compressive force in the steel section to the top of the steel section
d_3	= The distance from the centroid of the steel section to the top of the steel section
D	= depth of the steel section web
C	= the maximum longitudinal force carried by the deck for a partially composite beam
E_c	= elastic modulus of concrete
f'_c	= compressive strength of the concrete
F_p	= total radial force in the concrete deck at point of maximum live load plus impact moment
F_u	= tensile strength of shear stud
F_{yc}	= yield stress of the steel top flange

F_{yt}	= yield stress of the steel bottom flange
F_{yw}	= yield stress of the steel web
L_P	= distance along girder from the point of maximum moment due to live load plus impact to the point of zero moment
M_n	= flexural capacity of the composite beam
n	= minimum number of shear studs required between the point of maximum live load moment with impact and the adjacent point of zero moment
n_p	= the number of shear studs provided between the point of maximum live load moment with impact and the adjacent point of zero moment
P	= total nominal shear force
P_{1P}	= one of two limiting values for the total longitudinal force in the concrete deck due to live load plus impact
P_{2P}	= one of two limiting values for the total longitudinal force in the concrete deck due to live load plus impact
P_p	= total longitudinal force in the concrete deck due to live load plus impact
Q_n	= nominal shear resistance of an individual shear stud
Q_r	= factored shear resistance of an individual shear stud
R	= minimum girder radius over the length under consideration
t_{fc}	= thickness of the steel top flange
t_{ft}	= thickness of the steel bottom flange
t_s	= thickness of the concrete deck

t_w = thickness of the steel web

ϕ_{sc} = resistance factor for shear studs

Chapter 1: Introduction

1.1 Overview

Steel highway bridges today are most commonly built with a concrete deck on top of the steel girders and are typically designed to act compositely with the concrete deck. This composite style design means that the two systems, the steel girders and the concrete deck, are designed to act together under loading. This design style leads to more efficient bridge designs as it enables the steel girders to act primarily in tension under most loading conditions while the concrete acts in compression under most loading conditions, both of which are preferred for the given materials. In order to achieve this type of composite behavior, a mechanical connection between the concrete deck and steel girders is required. This connection is achieved using what are most commonly called shear connectors, as they function by allowing shear transfer between the steel and concrete.

The most common type of shear connector in practice today is the shear stud connector which is a headed stud that is attached to the top flange of the steel girder section by a drawn-arc welding process. This type of connector is shown in Figure 1.1-1. Once the deck is cast, the head and shaft of the shear stud become embedded in the concrete. The standard size for these types of connectors is 1" or smaller in shaft diameter with 3/4" and 7/8" diameter studs most commonly used.

To achieve the required connection strength between the concrete and steel sections, typically hundreds or even thousands on large projects of these connectors must be welded to

the top flange of the steel girder. The design strength of these connectors is in part based on the cross-sectional area of the connector. Large diameter studs are generally considered to be those studs with a diameter larger than 1". As the studs have a larger diameter, they would clearly also have a larger cross-sectional area which would imply the possibility that fewer numbers of these large diameter studs may be capable of developing the same capacity as a larger number of standard diameter studs. For example, the cross-sectional area of a single large diameter 1.25" stud is approximately equal to that of two standard 7/8" diameter studs.

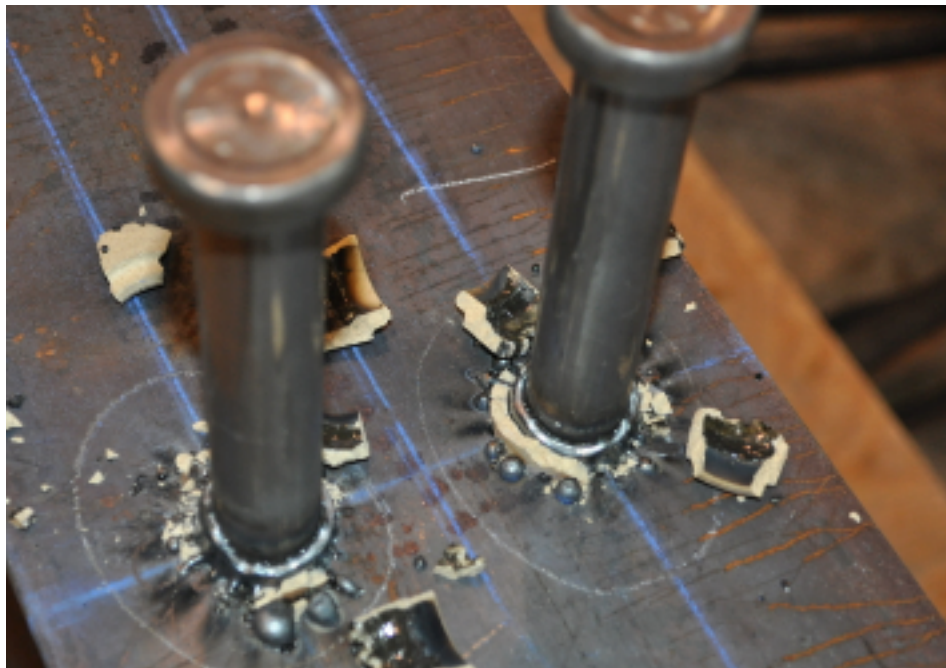


Figure 1.1-1: A pair of headed shear stud connectors welded to a steel flange

A potential reduction of this magnitude in the number of studs would be desirable for a number of reasons. As each stud must be welded onto the steel section, the number of welds

would be reduced. Having fewer studs would reduce the number of potential conflicts with the concrete deck reinforcement. Shear studs have been known to pose a tripping hazard to bridge workers in the field, so having fewer of them should reduce the risk of this type of accident. If a deck constructed with these large diameter studs needs to be replaced, there are fewer studs which must be removed. Despite these advantages, currently the AASHTO LRFD Bridge Design Specifications (AASHTO 2010) do not allow for these larger size studs to be used in highway bridges. This limitation is imposed due primarily to a lack of research and information on the performance of these large diameter studs in composite bridge construction.

1.2 Motivation

In the United States, a large number of bridges have reached or will soon reach their intended design lives. State Departments of Transportation (DOTs) across the nation are faced with an aging bridge inventory and highly constrained budgets coupled with construction time constraints based on congestion and traffic demands. Due to these constraints there is interest in saving both time and money by saving bridge superstructures that are still in good working order and replacing only the bridge deck. Even a deck replacement still takes time and forces at least partial shutdowns of major roadway traffic lanes, many of which are located in highly congested metropolitan areas. Therefore, rapid deck replacement is often paramount.

In the case of composite bridges, those with a steel superstructure supporting and acting compositely with a concrete deck, often hundreds or even thousands of shear stud connectors must be attached by a stud welding gun onto a steel superstructure after the old

deck is removed. Reducing the number of studs required would lower the amount of time required to apply shear connectors which in turn would reduce the overall time required to replace a bridge deck. To facilitate the use of fewer studs, it had been proposed to apply larger diameter shear studs. Using larger diameter studs would enable bridge fabricators to use fewer shear stud connectors while maintaining the same total cross-sectional area across all of the studs.

The time savings would come from the fact that the increase in welding time per stud would increase only slightly in switching to a larger diameter stud, but the number of studs required could be reduced by 50% or more. The potential time savings and corresponding reduction in economic costs due to traffic disruption essentially provide the motivation for this research.

This research effort was focused specifically on the performance of 1.25" large diameter shear studs. This stud size was selected as it appears to be the largest stud size that is compatible with the majority of shear stud welding equipment used in the field today. Sufficient research data has not been available to verify that large diameter studs designed under the current AASHTO LRFD Bridge Specification would perform adequately and safely compared to designs using a larger numbers of smaller shear studs in terms of both strength and ductility.

Prior work conducted at Auburn University by Mundie (2011) has verified the fatigue performance of the studs confirming that they safely meet the current AASTHO specifications. This work aims to establish the strength and ductility performance of large diameter shear studs

in composite bridge construction and confirm their compatibility with current AASHTO specifications for highway bridges or alternatively suggest new design specifications, ultimately enabling State DOTs the ability to utilize large diameter shear studs in applications which would benefit from their use.

1.3 Objectives

The Research for this project focused on accomplishing two key objectives:

- 1) Experimentally evaluate the strength and ductility of large diameter shear studs used in the construction of composite bridge structures.
- 2) Based upon experimental results, propose strength design recommendations for large diameter shear studs

1.4 Research Tasks

In order to carry out this research, several tasks had to be performed to ensure fulfillment of the research objectives. These tasks are listed below in the order in which the tasks were begun but not necessarily completed:

- 1) Identify research area of interest
- 2) Review existing design specifications, literature, and previous research
- 3) Develop an experimental concept and plan
- 4) Fabricate and prepare test specimens and loading equipment
- 5) Conduct experimental testing

6) Review and analyze experimental data

7) Propose recommendations for large diameter shear stud strength provisions

1.5 Scope and Approach

This research effort was focused on the strength and ductility of headed shear studs used in the construction of composite bridges and the applicable design provisions of AASHTO (2010). Other types of shear connectors found in composite bridge structures such as non-headed shear studs, bent studs, channels, etc. are not evaluated. The fatigue performance of headed shear studs and other applications of headed studs are also not within the intended scope of this project. Additionally the acceptability of other design specifications for use with large diameter studs is not considered within this project.

To provide a means of comparison, both standard 7/8" diameter and large 1.25" diameter studs were tested within this program so that a direct comparison can be made under the same specimen and loading configurations.

1.6 Thesis Organization

The research for this thesis has been organized into five chapters. The first chapter provides an introduction to the topic of shear studs in composite bridge construction, explains the specific motivation and objectives for this research effort, and explains the basic approach used to achieve the desired research goals. The second chapter provides additional background on large diameter shear studs and composite bridge construction, reviews existing strength

design provisions of AASHTO (2010), and then examines previous key research performed to date on the topic. Chapter 3 moves into the details of the testing program used for this research. It discusses the design, fabrication, and instrumentation of test specimens, the important material properties of test materials, the physical setup of the tests, and the specific protocol used to conduct each test. In Chapter 4, the results of all tests are provided and analyzed. In the last section, Chapter 5, the overall conclusions and implications of the research are indicated and discussed along with appropriate recommendations for continued advancement of the knowledge base for large diameter shear studs used in composite bridge construction.

Chapter 2: Background and Literature Review

2.1 Overview

Extensive research has been conducted on the strength of shear studs. This research has led to the present design criteria in AASHTO (2010) and in other standards worldwide. This section focuses on providing a basic understanding of the current strength provisions in AASHTO (2010) and the relatively limited research done thus far on the topic of the strength of large diameter shear studs and testing of full scale composite specimens.

2.2 Review of Current Design Provisions

This research focuses on evaluating the provisions in AASHTO (2010) and their applicability to static strength design of large diameter studs. Other research such as that by Shim, Lee, and Yoon (2004) which is discussed in more detail in the next section has evaluated the provisions of other international design codes such as Eurocode 4.

The provisions of interest for AASHTO (2010) begin in section 6.10.10.4. In this section, the factored shear resistance of a single shear connector is defined in equation 6.10.10.4.1-1:

$$Q_r = \phi_{sc} \cdot Q_n \quad (\text{EQ 2.2-1})$$

where:

ϕ_{sc} = The resistance factor for shear connectors specified as 0.85 in section 6.5.4.2

Q_n = The nominal shear resistance of an individual connector which is defined in article 6.10.10.4.3

The nominal shear resistance of an individual shear stud is defined in AASHTO (2010) according to Equation 6.10.10.4.3-2 as :

$$Q_n = 0.5 \cdot A_{sc} \cdot \sqrt{f'_c \cdot E_c} \leq A_{sc} \cdot F_u \quad (\text{EQ 2.2-2})$$

where:

A_{sc} = The cross sectional area of the individual shear connector (sq. in.)

f'_c = The compressive strength of the concrete (psi)

E_c = The modulus of elasticity of the concrete (psi)

F_u = The tensile strength of a shear stud connector (psi)

With the strength of individual shear studs defined by EQ 2.2-1 and EQ 2.2-2 given above, AASHTO (2010) then specifies Equation 6.10.10.4.1-2 which gives the number of shear studs required. Further, it indicates that this is the number of studs to be provided over the region from where maximum positive moment due to live load with impact is achieved to the adjacent point of zero moment. The equation is expressed as:

$$n = \frac{P}{Q_r} \quad (\text{EQ 2.2-3})$$

where:

P = The total nominal shear force using article 6.10.10.4.2

Article 6.10.10.4.2 of AASHTO (2010) considers two cases in defining the total nominal shear force. The first case is simple spans and continuous spans with non-composite behavior in regions of negative flexure while the second case deals with continuous spans which are composite in their final condition in regions of negative flexure. These cases are considered by Equations 6.10.10.4.2-1 and 6.10.10.4.2-5. As the first case, simple spans, is dealt with in this experimental effort, the first equation will be examined:

$$P = \sqrt{P_p^2 + F_p^2} \quad (\text{EQ 2.2-4})$$

where:

P_p = The total longitudinal force in the concrete deck at the point of maximum moment due to live load with impact as defined by the lesser of Equations 6.10.10.4.2-2 and 6.10.10.4.2-3

F_p = The total radial force in the concrete deck at the point of maximum live load plus impact moment as defined by Equation 6.10.10.4.2-4

The two controlling values for the total longitudinal force in the deck according to AASHTO (2010) equations 6.10.10.4.2-2 and 6.10.10.4.2-3 are given below. The minimum value given by the two equations is used as the total longitudinal deck force. The first equation clearly limits the longitudinal force based on the capacity of the concrete deck while the second equation limits the longitudinal force based on the capacity of the steel section. The equations are:

$$P_{1P}=0.85 \cdot f'_c \cdot b_s \cdot t_s \quad (\text{EQ 2.2-5})$$

$$P_{2P}=F_{yw} \cdot D \cdot t_w + F_{yt} \cdot b_{ft} \cdot t_{ft} + F_{yc} \cdot b_{fc} \cdot t_{fc} \quad (\text{EQ 2.2-6})$$

where:

b_s = The effective width of the concrete deck (in)

t_s = The thickness of the concrete deck (in)

and

F_{yw} = The yield stress of the web of the steel section

D = The depth of web of the steel section

t_w = The thickness of the web of the steel section

F_{yt} = The yield stress of the bottom flange of the steel section

b_{ft} = The width of the bottom flange of the steel section

t_{ft} = The thickness of the bottom flange of the steel section

F_{yc} = The yield stress of the steel section top flange

b_{fc} = The width of the top flange of the steel section

t_{fc} = The thickness of the top flange of the steel section

The radial force equation given in 6.10.10.4.2-4 of AASHTO (2010) for the concrete deck is based upon the longitudinal force in the deck and is given by:

$$F_P = P_P \cdot \frac{L_P}{R} \quad (\text{EQ 2.2-7})$$

where:

L_P = The distance from the end of the girder to the point of maximum moment from live load with impact

R = The minimum radius of the girder located within the length L_P under consideration

Collectively these equations from AASHTO (2010) control the strength design of shear connectors for use in composite bridges. The key assumption of the design philosophy implemented by AASHTO is the idea that the shear connectors have sufficient ductility to be able to redistribute load such that the localized spacing of shear studs relative to the localized shear intensity is not critical, only that the total number of shear connectors provided is sufficient to resist the total shear force at the interface between the steel and concrete sections. AASHTO does additionally limit the maximum stud spacing to 2 feet.

2.3 Previous Research

Slutter and Driscoll (1965)

Some of the earliest research into the ultimate strength of composite beams with shear studs was conducted by Slutter and Driscoll in 1965. Their test program consisted of twelve

simple span beam tests, one two span continuous beam test, and fifteen push-out type specimens. The test included a wide variety of shear connection types including friction only, bent studs, headed shear studs, and channel type connectors.

The researches investigated using plastic design approaches to design shear studs instead of the well established elastic design methods. According to results of the test, there was not a significant difference in terms of ultimate strength between beams with uniform stud spacing and non-uniform stud spacing conforming to the elastic shear diagram. This indicated that the shear connectors have sufficient ductility to redistribute load and that a plastic design approach was reasonable for composite beam design.

The researchers also focused on the effects of slip on beam performance. They concluded that when sufficient connectors were provided for full composite action, that the ultimate strength was not significantly affected by the magnitude of total slip of the deck relative to the steel section. Additionally, it was concluded that the overall beam deflection was not significantly higher in composite beams which experienced greater slip.

This research provided design recommendations which effectively became the basis of current AASHTO (2010) strength design provisions for shear studs. However, the largest headed stud tested as part of this testing program was 3/4" diameter. The researchers note that it appeared in specimens with larger diameter studs (3/4" as opposed to 1/2" diameter) , that the concrete experienced more localized damage, possibly weakening the beams. This, in part, is why the current provisions of AASHTO (2010) do not extend to large diameter studs.

Badie, Tadros, et al. (2002)

Recently, as state DOTs have begun putting more emphasis on rapid bridge and bridge deck replacement, some research has begun to investigate large diameter shear studs. In 2002, Baddie, Tadros, et al specifically began investigating large diameter studs, in particular the 1.25" diameter variety. This research initially looked at material properties for various stud materials and concluded that those used for other studs were suitable for use in large diameter studs.

The researchers performed twenty push-out type tests for ultimate strength testing, twenty-five push-out type tests for fatigue strength testing, one beam fatigue test in flexure, and then examined one full scale implementation of the large diameter studs in a bridge structure. In their strength testing regime, the specimens were broken down into four groups, one which used traditional 7/8" diameter studs, one which used 1.25" diameter studs in a comparable configuration, one which used 1.25" diameter studs mounted on steel sections that had been used for previous testing of 7/8" diameter studs which were removed, and then two groups which used both headed and headless large diameter studs. The results of the research indicated that an equal amount of 1.25" diameter studs provided roughly twice the capacity of the same number of 7/8" diameter studs and that the larger studs resulted in a reduction of slip by 30%.

A three span structure was constructed by the Nebraska Department of Transportation, with two spans having large diameter studs. Under a three axle dump truck load, no difference in deflection, or cracking tendencies were shown between the span using traditional studs as

compared to the two using large diameter shear studs. Further, the researchers note that they received comments from the contractor indicating that the presence of fewer studs on the girder increased the safety for workers.

The final conclusion of the researchers was that the AASHTO LRFD provisions of 1998 could be used to safely design large diameter studs and that the studs were able to achieve the goals of reducing the number of studs required to achieve composite action while reducing construction time and increasing safety. Additionally, the materials used and welding techniques in practice provide for sufficient stud performance. A minimum welding amperage of 2400 amps was recommended.

Shim, Lee, and Yoon (2004)

In 2004, Shim conducted additional push-out testing on specimens with large diameter shear studs. The testing program consisted of 25, 27, and 30 mm (0.98, 1.06, and 1.18") shear studs. The focus of this test was evaluating the strength and ductility of large diameter shear studs and comparing their performance with design codes, in this case Eurocode 4. The research concludes that, while the Eurocode 4 does not allow for large diameter shear studs similar to AASHTO (2010), that the design criteria are safe for the use of large diameter studs. The studs were found to provide adequate strength and ductility. It was indicated however, that after the peak load was obtained, the large diameter shear studs appeared to exhibit less ductility than standard diameter studs. Shim also concluded that satisfactory weld quality could be obtained for large diameter shear studs with minor modifications to existing automatic

welding equipment. The weld settings indicated to provide good quality welds were 2200 amps for 25 and 27 mm studs and 2400 amps for 30 mm studs. The weld duration used in each case was 1.3 seconds.

Lee, Shim, and Chang (2005)

In 2005 Lee, Shim, and Chang performed additional research on large diameter shear studs. In this experiment, the same three stud sizes as used previously by Shim, Lee, and Yoon (2004) for push-out specimen testing, 25, 27, and 30 mm (0.98, 1.06, and 1.18in.) diameter, were used again. This testing program consisted of nine push-out specimens used for static strength testing. Additionally, three composite beam specimens were fabricated, one for each size stud in the testing program. The beams were designed to have approximately 38% partial composite action. The top flanges of the specimens were greased to minimize frictional bonding at the steel to concrete interface. Weld conditions were also the same as those previously used by Shim, Lee and Yoon (2004) with 2400 amps at 1.3 seconds used for welding the large diameter studs.

The loading of the beam tests was performed at midspan in seven steps. Testing indicated that despite differences in the diameter and distribution of studs, that they all performed in a very similar manner in terms of load deflection behavior and ultimate capacity. They concluded based upon this, that the beam performance is controlled primarily by the degree of composite action achieved and did not depend heavily on the specific stud type, size, and configuration used. Also, all the stud diameters and configurations used provided adequate

strength and ductility and were safe to use with existing provisions of Eurocode 4. The researchers did suggest increasing the safety factor built into the AASHTO LRFD Specifications. Additionally, the researchers found, as has been shown by previous research, that the flexural specimens provided a shear strength 1.59 times higher than that indicated by the push-out test program, indicating that push-out specimens provide conservative estimates for the shear strength provided by shear studs.

Chapter 3: Test Program and Protocol

3.1 Overview

This chapter focuses on the experimental phase of this research effort. The overall specimen configuration and design are discussed in this chapter. Values of all relevant material properties are also provided. The fabrication methods for the specimens are presented along with the test set up and instrumentation of each specimen. Along with specimen information and general test setup, the specific procedures used for conducting each test and the loading protocol used on each specimen are provided.

3.2 Specimen Design and Configuration

Given the limited research done on large diameter studs and in particular large diameter studs tested in beam specimens, this experiment has focused on preparing and testing of multiple beam type specimens under flexural loading. Based on project constraints, four of these beam type specimens were prepared. The key project constraints were the available lab space and the capacity of the hydraulic loading system. The specimen designs selected were targeted to be as large and representative of an actual bridge structure as possible while still satisfying project constraints. Each was designed to feature slightly less studs than required for full composite action. To be realistic with real world bridge structures, the neutral axis of the specimen was designed to fall within the concrete deck under ultimate loading. The specimen designs to follow were configured to satisfy the design constraints and goals.

Two beams feature 1.25" large diameter studs, one with uniform stud spacing (Specimen 2), the other with the studs placed in pairs at double the pitch of the uniform spacing (Specimen 4). This was intended to represent the cases in which these studs would be applied, a normal composite beam with a cast in place deck and uniform spacing and a composite beam with precast deck panels with discrete pockets of shear studs. All large diameter studs were shot onto the center of the top flange to satisfy minimum thickness requirement for the stud welding process.

The remaining two specimens featured 7/8" diameter studs. This size was chosen as the combined cross sectional area of two 7/8" diameter studs is effectively the same cross sectional area of a single 1.25" diameter shear stud and 7/8" is one of the more commonly used standard diameter stud sizes. For the beams with the 7/8" diameter studs, the pitch between studs was identical to that of the large diameter studs except that in place of each large diameter stud there was a pair of studs positioned transversely across the width of the flange. Specimen 1 features uniform stud spacing with a 24" pitch while Specimen 3 features stud clusters at a 48" pitch. A transverse cross section view of each specimen type can be seen in Figure 3.2-1. A longitudinal cross section view of each specimen can be seen in Figure 3.2-2.

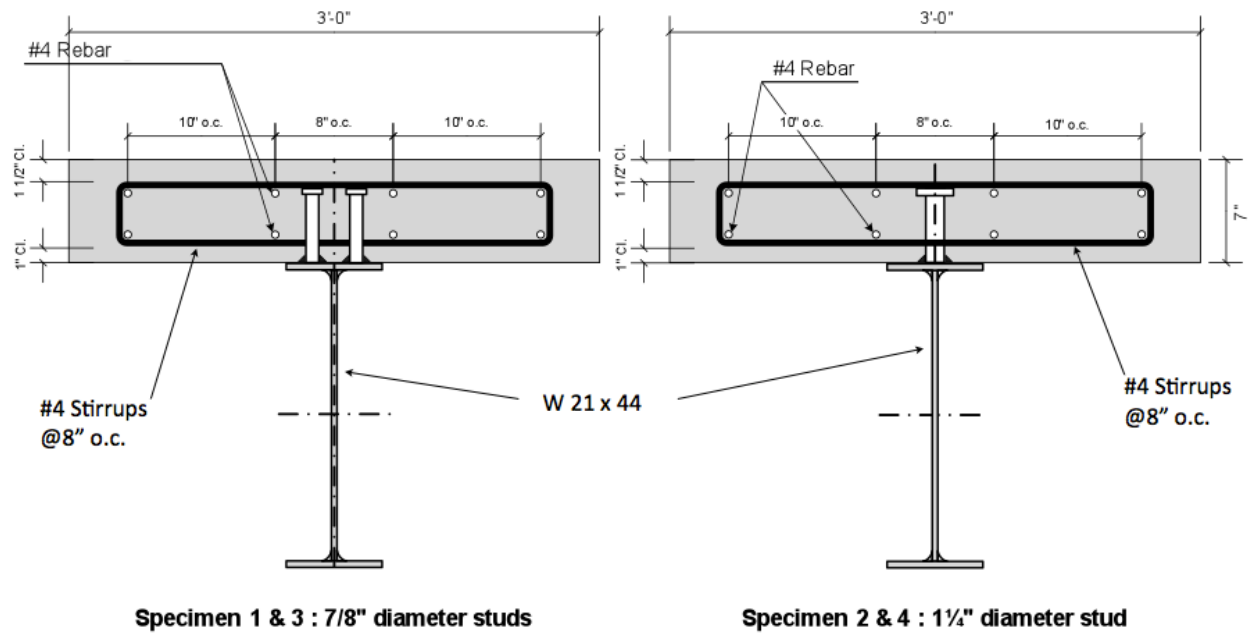
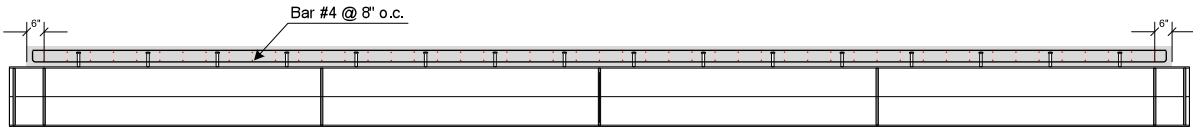
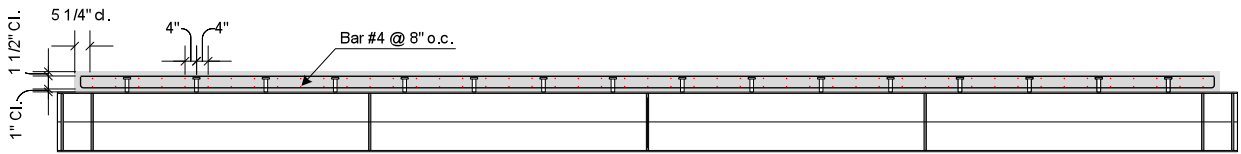


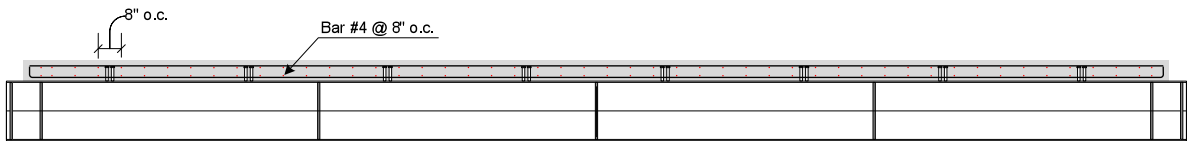
Figure 3.2-1: Transverse cross section view of specimen configurations



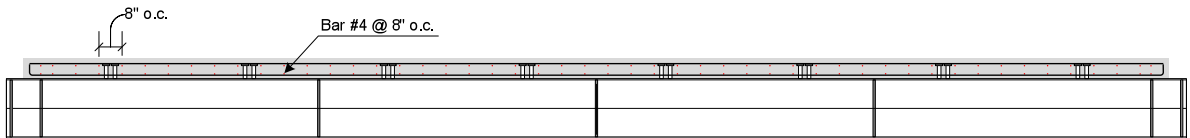
Specimen 1 : 34-ft long W21X44 Section ; 24" pitch, 7/8" diameter studs (total 32 studs)



Specimen 2 : 34-ft long W21X44 Section ; 24" pitch, 1 1/4" diameter studs (total 16 studs)



Specimen 3 : 34-ft long W21X44 Section ; 48" pitch, 7/8" diameter studs (total 32 studs)



Specimen 4 : 34-ft long W21X44 Section ; 48" pitch, 1 1/4" diameter studs (total 16 studs)

Figure 3.2-2: Longitudinal cross section view of specimen configurations

Each beam consisted of a rolled W21x44 structural steel section 34 feet in length with 3/4" thick bearing stiffeners welded on both sides at all reaction locations and their corresponding locations in unloaded regions, shear connectors, and a reinforced 7" thick, 36" wide concrete deck cast over the length of the steel beam except for a 6" region at each end of the beam to maintain access to lifting holes located in the steel section top flange. The reinforcement pattern was consistent for all specimens and was comprised of four #4 bottom

bars running the full length of the beam longitudinally with 1.5” of clear cover and four #4 top bars running the full length of the beam longitudinally with 2” of clear cover. The top and bottom bars were enclosed in #4 stirrups spaced uniformly on 8” on center. All reinforcement was Grade 60 rebar. The overall layout of the specimens may be seen above in Figures 3.2-1 and 3.2-2.

3.3 Material Properties

To properly understand the behavior and performance of the test specimens a number of material properties and dimensions were required. For the steel components of the test specimens, the W section test beam, the shear studs, and the reinforcing steel, certified mill test reports were used to quantify the key material characteristics of each of those components. Table 3.3-1 provides a summary of the key values obtained from material testing on the steel components.

Table 3.3-1: Steel Component Material Properties

Steel Component	Average Yield Strength (ksi)	Average Ultimate Strength (ksi)
W 21 x 44 Beam	58	72.5
7/8" Diameter Stud	52	65.8
1.25" Diameter Stud	77	85
#4 Rebar	69.3	106.2

The steel wide flanged beam was a standard rolled W21x44 section produced by Fab-Arc. The certified mill test report provided by the manufacturer gave two values for the yield strength and ultimate strength of this section. The indicated yield strength values were 59 ksi and 57 ksi. The indicated ultimate strength values were 73 ksi and 72 ksi. For all calculations used in this research effort, the yield stress of the steel beam sections has been taken as 58 ksi based on the average of values from mill testing. A copy of the mill test report for the steel beam section can be found in section A1.1 of Appendix 1.

The 7/8" diameter shear studs were provided by Nelson Stud Welding. Nelson Stud Welding conducted testing on 7/8" diameter studs from the production batch used and determined that the yield stress of the studs was 52 ksi. The ultimate strength was measured as 65.8 ksi. These values have been used in all subsequent analysis of the 7/8" diameter shear studs. The mill test report of the 7/8" diameter shear studs can be found in Section A1.2 of Appendix 1.

The 1.25" diameter shear studs were also provided by Nelson Stud Welding. They conducted testing on the 1.25" diameter studs from the batch produced for this research project and determined that the yield stress of this stud size was 77 ksi. The ultimate strength of the large diameter shear studs was found to be 85 ksi. These are the material characteristics that have been used in analysis of the beam tests. The mill test report for the large diameter studs is located in section A1.3 of Appendix 1.

The reinforcing steel was provided by Sabel Steel Service. All bars used in the deck reinforcement were standard #4 rebar. The certified mill test report provided by Sabel Steel Service showed a yield strength of 69.3 ksi and an ultimate strength of 106.2 ksi for this production batch. These are rebar material characteristic values that have been incorporated into subsequent calculations. The mill test report for the reinforcing steel can be found in Appendix 1, Section A1.4

Concrete properties are also critical to understanding and analyzing the experimental results so standard 4" by 8" test cylinders were cast for each concrete batch and tested at key time intervals. The cylinders were all air dried along side each test specimen. At each time interval, three cylinders were compression tested following appropriate ASTM guidelines. The complete log of each cylinder test can be found in Appendix 2 in Sections A2.3 and A2.4. A summary of key values obtained from these tests is provided in Table 3.3-2. The batch reports for the concrete are attached in Appendix 2, Sections A2.1 and A2.2. Specimens 1 and 2 were fabricated using concrete cast from Batch 1, while Specimens 3 and 4 were cast with concrete from Batch 2.

Table 3.3-2: Concrete Cylinder Test Compression Strengths

Batch 1	Age (days)				Specimen 1	Specimen 2
	7	14	28	92	190	219
	7 Day Strength	14 Day Strength	28 Day Strength	90 Day Strength	Test Day Strength	Test Day Strength
	4680	5170	5330	5260	4950	4640
Batch 2	Age (days)				Specimen 4	Specimen 3
	7	14	28	90	286	327
	7 Day Strength	14 Day Strength	28 Day Strength	90 Day Strength	Test Day Strength	Test Day Strength
	4370	5040	5220	4870	4800	4810

After the specimens were fabricated, they were carefully measured to determine the final as built dimensions. All steel thicknesses, where possible, were measured using a calibrated micrometer. Concrete dimensions, steel depths, and flange widths were measured using a conventional measuring stick. As all specimens were fabricated in the same manner with the same materials, differences were minimal between specimens, so the dimensions of each specimen were averaged to determine an overall set of values which could be used to analyze specimen performance. A summary table of these measurements is given in Table 3.3-3 for the steel components and Table 3.3-4 for the concrete deck. The diameters of installed shear studs are given in Table 3.3-5.

Table 3.3-3: Steel Component Measured Dimensions

Steel W Section Component	Thickness (in)	Width (in)	Overall Depth (in)
Top Flange	0.4326	6-5/8	20-9/16
Bottom Flange	0.4286	6-5/8	
Web	0.3585		
Bearing Stiffener	0.7553		

Table 3.3-4: Concrete Deck Measured Dimensions

Concrete Deck Cross-Sectional Properties	
Deck Width (in)	Deck Thickness (in)
35.97	7.10

Table 3.3-5: Shear Stud Measured Diameters

Nominal Stud Size	Measured Stud Size
7/8"	0.867"
1.25"	1.252"

3.4 Specimen Fabrication

After the 4 steel girders were delivered to the laboratory, the first significant fabrication task was to weld the shear studs onto the beams. A standard welding machine, in this case the Nelweld 6000, and gun were used. The large diameter shear studs did require a modification to

the cradle portion of the gun to appropriately fit the stud heads. Figure 3.4-1 shows an image of a large diameter stud being welded to the top flange with the welding gun and modified cradle. All of the studs were welded onto the top flange of the steel sections under the supervision of two representatives of Nelson Stud Welding, the manufacturer of the studs, welding gun, and welding machine, to ensure proper technique and weld quality. As no industry standards exist for welding large diameter studs, a number of test studs were shot to determine the optimal weld settings. Based on the test welds, 2500 amps with a duration of 1.5 seconds was the optimal setting. Bend tests were also conducted with all test studs bent to nearly 90 degrees or to the extent possible without failing, further indicating good weld quality. Figure 3.4-2 shows a representative high quality weld on one of the large diameter studs welded onto a test specimen.



Figure 3.4-1: A stud welding gun with modified cradle welds a large diameter shear stud to the top flange of a test specimen



Figure 3.4-2: A typical high quality weld of a large diameter stud on a test specimen

Following stud welding operations, form construction was the next major project task. To ensure direct comparability of the large diameter studs to the conventional stud size, the beams were cast two at a time with a large diameter specimen and a conventional specimen with the same stud pitch done in each pair. The beam and overhanging portion of the deck were fully supported and shored during casting and for a period of at least seven days following the pour date. The forms were constructed of wood and the concrete to wood interface was treated with form release agent. Form release agent was also applied to the top flange of the steel section to prevent frictional bonding from influencing interface slip data during the testing. During the application of form oil, the shear studs were covered in plastic which was then removed before casting took place. Figure 3.4-3 shows a view of the concrete formwork assembled with two test beams in place.



Figure 3.4-3: Fully assembled concrete formwork

The reinforcement cages for the concrete deck were assembled inside the forms. The deck reinforcement consisted of four bottom bars running longitudinally with a 1.5" clear bottom cover, four top bars running longitudinally with a 2" clear top cover, and stirrups enclosing the longitudinal bars spaced at 8" on center. All reinforcement consisted of Grade 60 #4 bars. The reinforcement cages were built on 1.5" rebar chairs and were connected using steel wire ties.

For the concrete, standard ALDOT mixture AF1C without ADVA was used for both pairs of beams. For the casting operation, concrete was loaded from the delivery truck to an overhead hopper which then was used to fill the forms. A view of the casting operation can be seen in Figure 3.4-4. The concrete was vibrated and then troweled smooth. A set of standard 4" by 8" test cylinders was also cast with each set of beams. The cylinders were ambient cured and then tested at 7, 14, 28, and 90 days as well as within 24 hours of each specimen test.

The first pair of beams was cast and then allowed to cure for at least the minimum prescribed time of seven days. During curing, the specimens were covered in wet burlap which was then covered in heavy plastic wrap. Once curing was complete, the composite beams were lifted vertically out of the forms. The first pair of beams was stored off to the side, then the second pair of steel beams were lowered into the forms and the same process was followed again to cast this second pair of beams.



Figure 3.4-4: Casting of concrete deck from overhead hopper

3.5 Test Setup

The beam was designed to be loaded by two hydraulic actuators, one at midspan and another at quarterspan. The load was to be applied onto the specimen through a 12" square, 1.5" thick 90A polyurethane pad with a 2" steel plate on top of it. The actuator head had a 1" thick, 12" square steel plate mounted onto it. A 1/8" thick high strength rubber traction mat was placed at the interface of the 2" thick plate and the 1" thick plate of the actuator head.

This assembly can be seen below in Figure 3.5-1.



Figure 3.5-1: Load application system under actuator

Two reinforced concrete pedestals were fabricated for supports at each end. A layer of high strength self-leveling epoxy was applied to the top surface of the pedestals to ensure a level support surface for the beam. A 1/8" thick high strength rubber traction mat was placed on the epoxy surface, then a 1.25" thick, 12" square A 514 steel plate with milled surfaces was centered on top of the pedestal. On top of the plate sat a polished 6" diameter, 12" long steel cylinder.

For the support on the loaded half of the beam, this cylinder was designed to act as a roller, allowing rotation and longitudinal translation of the beam at the support location. This assembly may be seen in Figure 3.5-2. At the other end, two appropriately shaped wedges were positioned on each side of the cylinder to create a pin connection which would enable the specimen end to rotate but not translate. These wedges were then clamped in place using high strength clamps. This assembly can be seen in Figure 3.5-3. Note that in this figure, the full clamping system is not in place to enable a clear view of the cylinder and wedges.



Figure 3.5-2: Roller support assembly and stability bracing



Figure 3.5-3: Pin support assembly

Another 1.25" thick, 12" square A 514 steel plate with milled surfaces was mounted to the bottom of the bottom flange of the beam at the appropriate support location. This plate was attached by a pair of steel angle sections on each side which were bolted to the steel plate on bottom and to the bearing stiffener at the top. This increased the bearing area and stabilized the specimen from tipping laterally as the nominal bottom flange width was somewhat narrow at 6.5". This assembly can be seen in Figure 3.5-2. To further ensure specimen stability, anchors were drilled into the edge of the beam slab and the concrete pedestals and then high strength cargo straps were connected between the anchors, but not tensioned, such that if the specimen did begin to tip, the straps would tighten and restrain excessive undesired movement. This set up can be seen in Figure 3.5-4.



Figure 3.5-4: Support strap safety system

3.6 Instrumentation

The loading protocol calls for the specimen to be loaded at quarterspan and midspan. The other half span was not loaded. The loaded half span is fully instrumented. The entire beam was fitted with draw wire type vertical displacement sensors mounted to the bottom flange of the steel section every 4 feet under the beam centerline. At the support locations and

the quarterspan and midspan cross sections, draw wire sensors were also connected 3.5" from the edge of the concrete slab to indicate any potential twisting of the beam. These sensors can be seen on the specimen in Figure 3.6-1. The overall layout of these sensors as well as the piston type displacement sensors and laser type optical displacement sensors can be seen in Figure 3.6-2 below.



Figure 3.6-1: Draw wire vertical displacement sensor

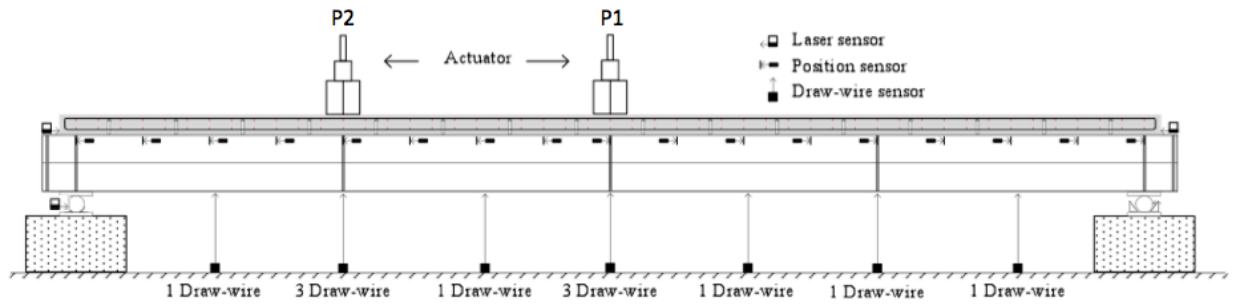


Figure 3.6-2: Draw wire, laser, and piston type (position) displacement sensor layout

Piston type displacement gages were mounted every 2 feet along the length of the beam onto the bottom of the top flange on both sides of the specimen. Contact blocks were then mounted onto the bottom of the concrete slab at these locations. These blocks were positioned such that the piston from the displacement sensors contacted the target block and were at approximately midstroke for the piston displacement sensor. This configuration was designed to detect relative slip between the steel and concrete section after each stud or pair of studs. This type sensor, the mounting block, and contact block configuration can be seen in Figure 3.6-3. The mounting block and contact block were attached with adhesive to the steel and concrete respectively and were shaped such that their centroidal axes aligned as nearly as possible. The overall layout of these piston type displacement sensors can be see above indicated as Position sensor in Figure 3.6-2.



Figure 3.6-3: Piston type sensor with mounting block and contact block

As slip at the steel to concrete interface was critical in assessing shear stud performance, laser type optical displacement sensors were also used to measure slip, in this case the cumulative slip over the entire length of the beam. The laser transmitter/receiver unit was mounted to the top of the top flange in the 6" region at the end of the beam where the concrete deck was terminated. One such sensor was mounted at each end of the specimen. A reflective target was then mounted on the concrete on the end of the slab. This instrumentation configuration can be seen in Figure 3.6-4. One additional laser sensor was mounted on the concrete support pedestal and targeted to the cylinder on the roller end of the specimen to monitor longitudinal translation. The overall layout of these laser type optical displacement sensors can be seen above in Figure 3.6-2.



Figure 3.6-4: Laser displacement sensor and target

The other type of sensor used is the electrical resistance strain gage. Strain gages were utilized in four cross-sections in the loaded half span of the bridge. Between these four sections there were two typical sections with consistent instrumentation patterns, referred to as sections A and B. At all four sections, two high elongation strain gages were used on the bottom of the bottom flange while two more high elongation strain gages were used on top of the bottom flange. Additionally one gage was installed on each side of the web at mid-depth. This was the entire strain gage array at typical cross section B which was at quarterspan and midspan. Typical cross section A featured additional gages and was located at the 1/8 and 3/8 span locations. At these sections, there were two additional strain gages on the bottom of the top flange. Two more gages were installed on top of the top flange with a special protective coating

before deck casting. These sections also featured two concrete strain gages on bottom of the slab with two more on top of the slab. A schematic of the two typical cross sections can be seen in Figure 3.6-5.

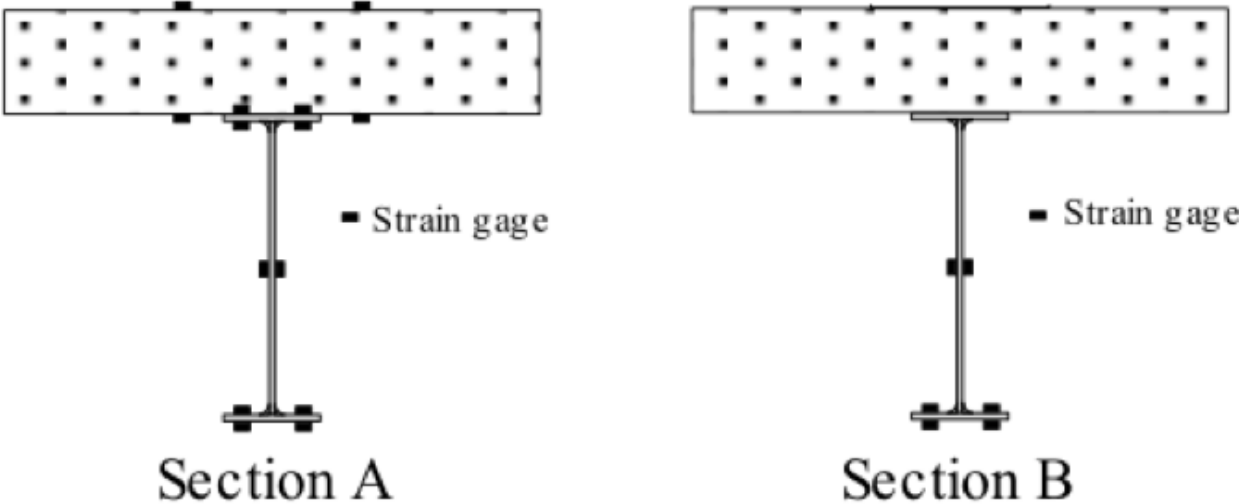


Figure 3.6-5: Typical strain gage cross section patterns

In addition to the various sensors mounted to the test specimen, force and displacement data was also collected from the output of each hydraulic actuator. In total, ninety-six channels of data were collected and recorded through the laboratory acquisition system. Each of these channels was sampled at 100 times per second.

3.7 Loading Protocol

For each beam, an initial set of testing was done to verify specimen stability and alignment as well as to trouble shoot any instrumentation difficulties. During this testing a maximum load of up to 35 kips was gradually applied and then removed at midspan only. This process was repeated three times. During this process, data was sampled at 10 times per second. After the initial round of testing, the data was analyzed to verify that all channels were recording correctly and that the specimen was behaving in a manner consistent with expectations.

For the primary test, the load application procedure was more complicated as both hydraulic actuators, one at midspan and one at quarterspan had to be used. To accomplish this test, two methods of actuator control were implemented. The first type of control, referred to as load control, has the user specify a load value, which the actuator will apply and maintain regardless of the displacement of the loaded object. The second type of control used, referred to as displacement control, has the user specify an actuator head displacement value. In this instance the actuator will move to, then hold a set location, regardless of the force required to maintain that position. The load configuration used during the experiment can be seen below in Figure 3.7-1 along with the resulting moment diagram for this loading pattern.

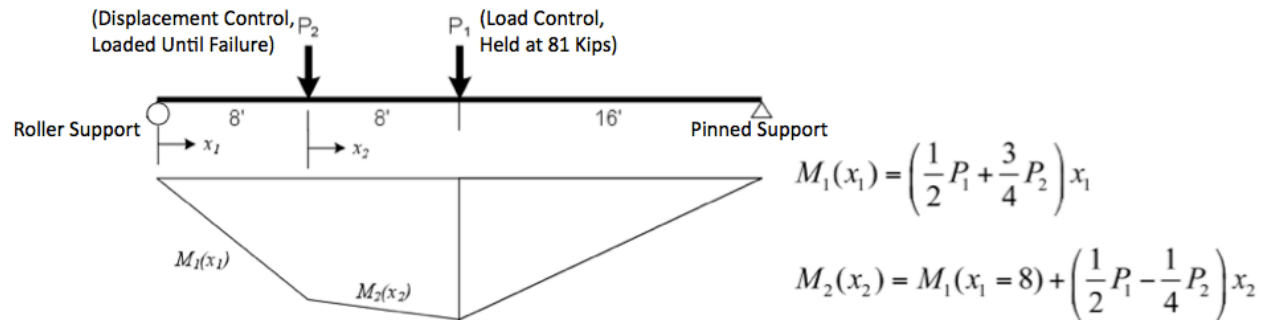


Figure 3.7-1: Loading configuration and moment due to applied loads diagram

For this test, the first actuator and its corresponding load value, referred to as P_1 , were applied at midspan under load control. During this portion of the test, the second actuator located at the beam quarterspan was not powered up and was not applying any load to the specimen. The load value from the midspan actuator was gradually raised in 10 kip intervals at an approximate loading rate at or less than 4 kips per minute. This was done till the actuator reached its maximum applied load for the test which was 81 kips. This load was held and maintained for the duration of the test until failure of the specimen.

For the 2nd actuator and its corresponding applied load value, referred to as P_2 , displacement control was utilized. As was done previously, the load was applied gradually in 10 kip increments. In this case, a 4 kip per minute or less loading rate was also targeted, however, this was more of an approximation since for this actuator the applied load itself was not directly controlled as it was under displacement control. The load rate was particularly difficult to

maintain in the later portions of the test when the specimen stiffness decreased due to nonlinear behavior.

This loading procedure was followed until specimen failure was observed as determined by specimen inability to support increased loads. This loading procedure enabled for post peak behavior to be captured as the additional applied load would all be under displacement control. It also enabled for three regions of different loading behavior. Between P2 and the roller support there would be a region of high shear and low moment. Between P1 and P2 there would be a high moment, low shear region, and between P1 and the pinned support there would be an intermediate shear, intermediate moment region. This enables the effect of load condition on stud performance to be assessed.

Chapter 4: Results and Data Analysis

4.1 Overview

This chapter focuses on presenting and analyzing the findings of the experimental portion of this research project. Specifically, it will discuss the sign conventions used for the presentation of results and calculations. It will provide a partial composite action analysis of the performance of each test specimen. A qualitative assessment of key observations from the fabrication and experimental phases of the project will be made. Finally, the collected experimental data is presented and analyzed.

4.2 Numerical Sign Conventions

To the extent possible, a consistent sign convention in terms of reference axis and positive and negative magnitudes, has been used for each data type in all figures, tables, and calculations. Selection of the specific sign convention used for each data type was based on convenience, clarity of results, and consistency with normal engineering and research practice.

Strain measurements have adopted a sign convention based upon compression and tension. Strains which correspond to longitudinal tension in the surface the gages are bonded to have been defined as positive. Strains which correspond to longitudinal compression in the surface the gages are bonded to have been defined as negative. All strain gages were aligned parallel to the longitudinal axis of the specimen to measure only longitudinal strains.

Displacements have been defined in terms of one vertical axis and one horizontal axis. For the vertical axis, as only downward deflections were anticipated based on the experimental configuration, for convenience vertical displacements have been defined as positive downward or with gravity while negative has been taken as upward or against gravity. For horizontal displacements, the reference axis has been taken as the longitudinal direction for the test member. Based on the anticipated movement of the member at the roller supported end of the beam, positive has been defined as movement from the pinned support, on the unloaded half of the beam, toward the roller support in the loaded half of the beam. Negative has been defined as movement in the opposite direction or from the roller end of the beam toward the pinned end of the beam.

For slip measurements, all movement is computed relative to the steel section. Therefore, the steel section is the reference point for all slip measurements which then are based on the distance that the concrete slab has moved relative to the steel section. The sign convention of this movement, measured in the longitudinal direction for the beam specimens, has been taken as the same as described previously for displacements along a horizontal axis. Positive is therefore defined as movement of the concrete slab relative to the steel section from the pinned end, toward the roller supported end. Negative has been taken as movement of the concrete slab relative to the steel beam from the roller support end, toward the pinned supported end.

Measurement of applied moments is based on the type of strain experienced in the bottom flange of the steel section for the composite beams. Moments which induce tensile

strain in the bottom flange of the steel section are considered as positive. Applied moments which induce compression into the bottom flange of the steel section are described as negative.

4.3 Partial Composite Action Analysis and Results

All of the specimens designed and used as part of this test program were designed to be partially composite, meaning that the total strength capacity of the shear studs is less than that required for the specimen to reach its theoretical moment capacity with the steel and concrete fully working together. Under this type of design, the capacity of the shear studs would therefore limit the capacity of the specimen. To characterize specimen performance and in particular shear stud performance, it is therefore necessary to perform computations for partially composite type beams to accurately assess the performance relative to theoretical expectations. As the different size shear studs provided by the shear stud manufacturer had different material properties, a partial composite action analysis also enables for the beams with different size shear studs to be directly compared to one another by normalizing the results based on the degree of composite action or DOCA.

The degree of composite action for partially composite members is essentially the ratio of the strength of the connection provided by shear connectors to the strength of shear connectors required for full composite behavior. In practice, it may be computed by examining the region from the point of maximum positive moment due to live load plus impact to the

adjacent point of zero moment. Taking Q_n from EQ 2.2-2 and P_p from the minimum of EQs 2.2-5 and 2.2-6, it is then determined by the equation:

$$DOCA = \frac{n_p Q_n}{P_p} \quad (\text{EQ 4.3-1})$$

where:

n_p = The number of shear studs provided from the point of maximum positive moment to the adjacent point of zero moment

Using the provisions of *AISC Specification for Steel Buildings* (AISC 2010), the capacity of a partially composite beam may be determined. AISC 2010 provisions are used in this case because AISC 2010 specifically addressed partial composite beam design where AASHTO (2010) encourages the use of full composite designs. The same plastic design theory and formulation to determine the flexural strength of the beam are employed in both cases. Determining the theoretical capacity of the partially composite beams used for this experiment will enable experimental beam performance to be compared to an expected value. This level of performance may then be used to compare specimens with differing DOCA values.

To do this, AISC 2010 introduces a third controlling value for the maximum longitudinal force carried by the deck to P_{1P} and P_{2P} which were previously discussed in Section 2.2. According to AISC 2010 the maximum longitudinal deck force would be the minimum of the

three values but in the particular case of a partially composite beam, the shear studs will be the limiting value such that this force is given by AISC 2010 Equation C-I3-8:

$$C = n_p \cdot Q_n \quad (\text{EQ 4.3-2})$$

Using that value for the longitudinal force carried in the deck with b_s and f_c' as discussed in Section 2.2, AISC 2010 then defines the depth of the equivalent stress block in the concrete in Equation C-I3-9:

$$a = \frac{C}{0.85 \cdot f_c' \cdot b_s} \quad (\text{EQ 4.3-3})$$

The moment capacity for the beam is then provided in Equation C-I3-10 of AISC 2010 as:

$$M_n = C(d_1 + d_2) + P_{2P}(d_3 - d_2) \quad (\text{EQ 4.3-4})$$

where:

d_1 = The distance from the centroid of the compressive force in the concrete deck to the top of the steel section

d_2 = The distance from the centroid of the compressive force in the steel section to the top of the steel section. It is taken as zero if there is no compressive force in the steel section

d_3 = The distance from the centroid of the steel section to the top of the steel section

Using these equations, the degree of composite action and theoretical moment capacity of each test beam can be determined. Table 4.3-1 provides the specimen configurations and

DOCA. Table 4.3-2 provides the experimental and theoretical moment capacities of each specimen. The experimental moment values included in are tabulated on the basis of applied moments and dead loads have been accounted for by subtracting from the theoretical capacity. For the 1.25" diameter studs, the stud strength from EQ 2.2-2 was controlled by the concrete strength while the 7/8" diameter studs the stud strength was limited by the steel strength term.

Table 4.3-1: Specimen Configurations and Degree of Composite Action

Test Specimen	Nominal Stud Diameter (in)	Stud Spacing (ft)	Degree of Composite Action (%)
1	0.875	2	84.10
2	1.25	2	89.43
3	0.875	4	84.10
4	1.25	4	91.74

Table 4.3-2: Theoretical and Experimental Moment Capacities

Test Specimen	Experimental Moment Capacity (kip*ft)	Theoretical Moment Capacity (kip*ft)	Experimental / Theoretical (%)	Percent Difference (%)
1	864	854	101.2	-3.4
2	870	856	101.6	-2.8
3	822	851	96.6	-7.7
4	849	864	98.3	-6.0

The large diameter studs in both patterns have outperformed or equaled the performance of the ordinary studs in terms of flexural capacity. In comparing Specimens 1 and 2, the beam with the large diameter studs had a higher experimental capacity, which was expected given the higher ultimate tensile strength of the large diameter shear studs. The same trend is even clearer in comparing Specimens 3 and 4. The specimen with large diameter studs again had a larger experimental capacity.

However, that result was expected, given that the two specimens with large diameter studs had higher theoretical capacities than the corresponding specimens with normal diameter studs. When comparing each specimen's theoretical capacity to its experimental capacity, the large diameter studs still performed slightly better. Between Specimens 1 and 2, Specimen 2 achieved 0.4% more of its theoretical capacity. Between Specimens 3 and 4, Specimen 4 with its large diameter studs achieved 1.7% more of its theoretical capacity. These differences, while modest, do indicate that the large diameter studs used in composite bridge construction do provide a flexural strength capacity comparable to that of standard diameter shear studs.

In comparing the beam configurations with uniformly spaced shear studs to those with more widely spaced stud clusters, the beams with closer, uniform spacing appear to achieve a higher percentage of the expected theoretical strength. This does suggest that the spacing and distribution of studs does have an effect on the ultimate capacity of the beam although that difference would appear to be small.

A key indicator of specimen ductility is the ability of the shear studs to redistribute load, which the studs would be forced to do in the configuration with more widely spaced clusters. A

higher flexural capacity in the case of a partially composite beam would in this case indicate better ability to redistribute loads and in turn, a higher degree of ductility exhibited by the shear studs. As was previously noted, the specimen with large diameter shear studs does achieve a higher experimental flexural capacity and a higher percentage of its theoretical flexural capacity than the specimen with standard diameter studs. It may also be observed that in comparing Specimens 1 and 3, 4.4% less of the theoretical capacity was achieved in the latter. In Specimens 2 and 4, those with large diameter studs, this reduction was less at 3.1%, which serves as another positive indicator of the large diameter studs ability to exhibit ductility under flexural loading to an extent equal that of smaller diameter studs.

The same plastic design methodology used to determine the capacities of beams designed with standard diameter studs also appears to be equally valid in the case of large diameter studs. In terms of strength capacity and ductility, there is no evidence that the plastic design methodology employed by AASHTO (2010) would not be safe to use with large diameter studs when applied with the appropriate load and resistance factors employed by the specification.

4.4 Qualitative Observations and Analysis

Welding Process and Fabrication

Several key conclusions not numerically captured by any collected data can be established. One aspect not explicitly addressed is the feasibility and practicality of using large

diameter shear studs in practice. The researchers, with supervision from representatives of Nelson Stud Welding, performed welding for all specimens in the lab specifically to be able to assess and identify any issues associated with the welding process.

To start the welding process, a modification to the stud cradle portion of the welding gun was necessary for the large diameter studs as was previously seen in Figure 3.4-1. The modification was done with parts provided by Nelson Stud Welding and completed with readily available standard tools in the laboratory. The process took approximately 1 hour. As this was the first time that the researchers or Nelson Stud Welding personnel had ever done this modification, it is reasonable to assume that, with wide implementation of large diameter studs, that this modification procedure would be standardized and could be performed quickly.

The modified cradle did noticeably add to the weight of the welding gun. As this was the first use of this type of cradle, its bulk was primarily due to a heavier, more conservative design which could certainly be refined in the future. After viewing the operation, it is reasonable to conclude that the cradle modification when introduced and mass produced could be refined to the level of the standard cradle portion of the gun, such that the weight of the gun for large diameter studs would not be a concern for reducing welding speed.

Once the modification was complete, weld quality was the next source of concern. Trial welds were performed to determine the optimal setting for welding the large diameter studs. Based upon visual inspection, 2500 amps at 1.5 seconds was found to be the optimal setting. One difficulty with the large diameter studs was actually testing the weld quality. The studs were bent to the degree possible and showed no signs of weld or stud failure under a 90 degree

bend test. However, they could only be bent a nominal amount, around 30 degrees. Therefore, it would be necessary to develop a new method besides 90 degree bend tests to examine weld quality in the field. Alternatively a new set of guidelines for performing bend tests on large diameter shear studs could be developed. On a holistic basis, based on bend tests and visual inspections, a consistent high weld quality was obtained throughout the welding process for both the large diameter shear studs and the normal 7/8" diameter shear studs using the Nelweld 6000 system.

The final area of concern with the welding operation was the welding time for the large diameter studs compared to standard sized studs. One of the presumed advantages of the large diameter studs was the ability to reduce the time of the welding operation to allow for more rapid bridge deck replacement. With the slightly longer weld time and heavier weld gun configuration, each weld performed on a 1.25" diameter stud did take longer than the corresponding weld of a 7/8" diameter stud, however as was discussed previously, only half the number of welds were actually required. In total, factoring in weld gun set up time, test welds, settings adjustments, etc., the total time used to conduct all welding operations on the 1.25" diameter studs was very similar to the time to conduct all welding operations for the 7/8" diameter studs. In terms of the actual time of welding only, the 1.25" diameter studs were attached more quickly as the time savings of performing half as many welds did outweigh the slight increase in time to weld each individual stud. Given that the number of studs required for this research effort is quite small compared to many bridge projects and that the setup procedure for the large diameter studs was experimental, it is reasonable to conclude that on a

larger highway bridge project, with an established set up procedure, the time of the welding operation would be more dramatically reduced by the use of large diameter studs as compared to what was seen in the laboratory.

Experimental Testing

From the standpoint of visual observations, all of the test specimens performed remarkably similarly. The same basic response sequence was seen in every test. First, the beam would deflect under the load at midspan. Aside from the deflection itself, there were no visible signs of distress. The deflection of a specimen under full load at midspan and no load at quarterspan can be seen in Figure 4.4-1.



Figure 4.4-1: Beam specimen under load at midspan

As the magnitude of loading increased and additional load was applied at quarterspan, the deflections of each specimen continued to increase but there were no readily observable signs of distress, again, other than the deflection itself. This was the case for each of the test specimens. The increased deflection of the beam specimen under full load at midspan and an increased load at quarterspan can be seen below in Figure 4.4-2.



Figure 4.4-2: Deflection of beam specimen under load at midspan and quarterspan

As the specimens continued to progress through the loading protocol, the first signs of distress began to appear in the web of the steel section at midspan. As yielding progressed up through the web, the pattern of striations occurring in the 45 degree cross hatched pattern shown in Figure 4.4-3 could be seen. By the end of the test, this could be seen at midspan over the full depth of the web and in the web near the bottom flange of the section at quarterspan. The extent of this pattern on the steel section can be seen in Figure 4.4-5.



Figure 4.4-3: Striations visible in web of steel section at midspan

Additionally, along with the pattern of striations in the web, material from the bottom of the bottom flange began to fall and accumulate on the floor. This pattern of small flakes of what appeared to be black material falling and accumulating under the beam was first visible under midspan and then eventually under quarterspan as well, as oxides and other materials attached to the surface of the steel section began to flake off under the increased material deformations of the steel section. An image of these flakes of material on the laboratory floor under a beam specimen at midspan can be seen below in Figure 4.4-4.

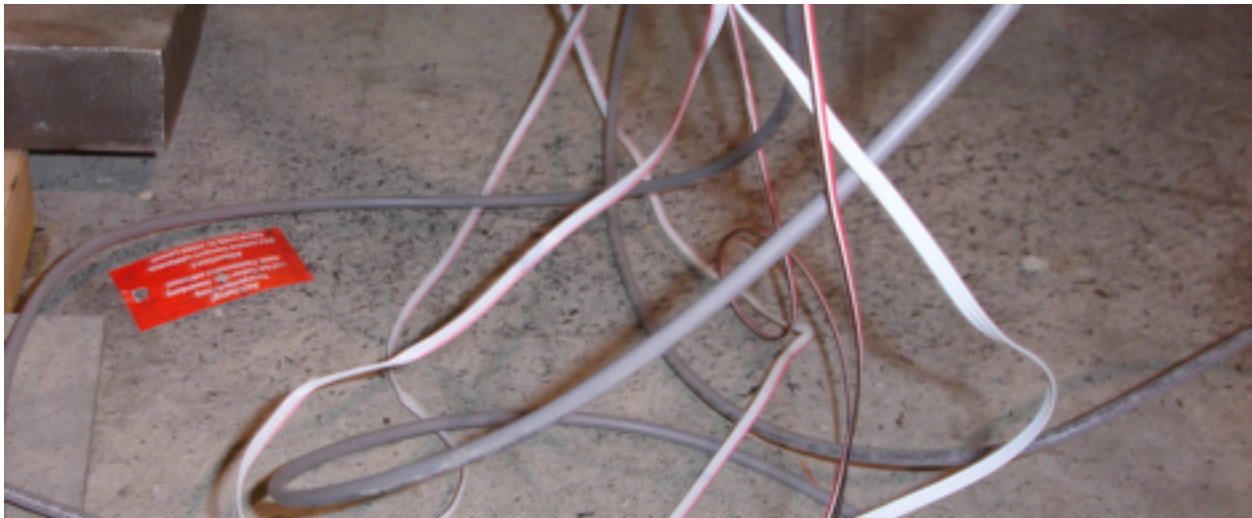


Figure 4.4-4: Flakes of surface material from the steel section accumulating under the specimen

After the specimens began to show signs of distress in the steel section, no additional obvious signs of severe distress were seen in the test specimens until right before the onset of failure. As failure approached, occasional noises could be heard from the test specimens.

Qualitatively, it was observed that these noises were more pronounced in Specimens 3 and 4 with the larger stud spacings. However, no visual sights accompanied these noises, so it is difficult to assess their meaning. As the peak load was reached, the first sign of failure to appear was tension cracking in the bottom of the concrete deck near midspan. As the specimen continued to be loaded, the number and size of these cracks continued to increase. They were all centered near the midspan portion of the beam and were, by the end of the test, seen at several feet either side of midspan. These cracks did not appear in the quarterspan region. A flexural tension crack forming in the bottom of the concrete deck can be seen below in Figure 4.4-5. Concrete cracks have been traced with black permanent marker.

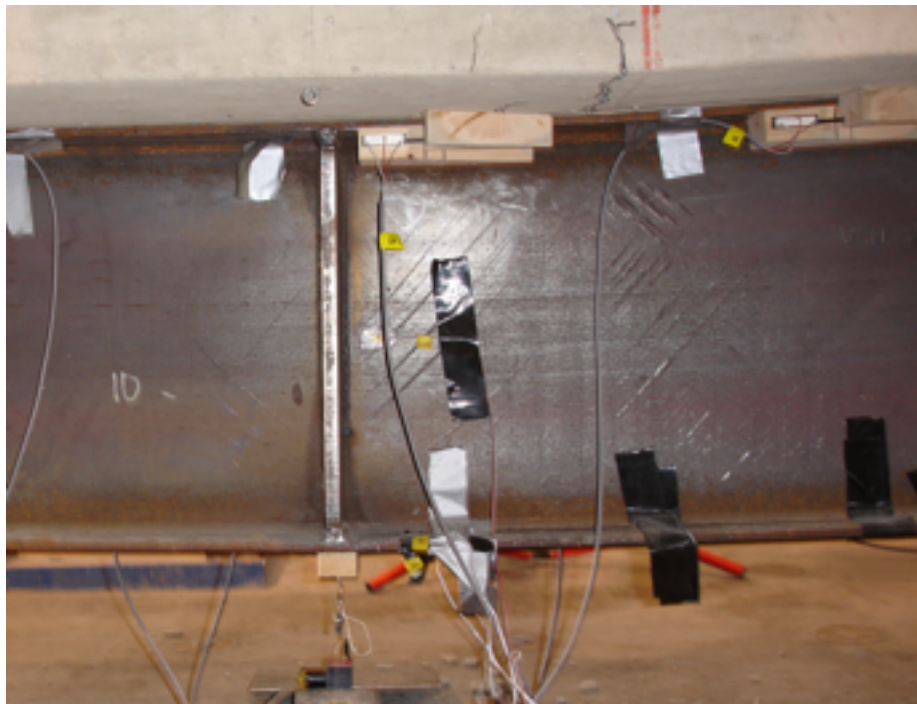


Figure 4.4-5: Tension cracks forming in the bottom side of the concrete deck at midspan

Almost immediately after flexural cracks began forming in the bottom of the concrete deck, the concrete began to crush in the top surface of the concrete deck. This was exhibited not precisely at midspan, but immediately adjacent to the location of load application at midspan. For each test specimen, the location was the same. This was always exhibited next to the actuator at midspan, on the side nearer the load at quarter span. The result of this crushing on top of the deck and cracking on bottom of the deck can be seen below in Figure 4.4-6 for Specimen 1.



Figure 4.4-6: Crushing at top of deck and cracking at bottom of the deck for Specimen 1

Once this crushing of concrete at the top of the deck started, the total load levels began dropping while the deflections rapidly increased. Once this began to occur, the specimens were considered to have failed. However, Specimens 1 through 3, were loaded until the actuator at midspan reached its maximum stroke capacity of 10" and the beam could be loaded no further. Specimen 4 was loaded until failure, but the test was terminated before the midspan actuator was fully extended due to a concern with a loose hydraulic control cable. The typical deflected shape of a test specimen after failure was reached can be seen in Figure 4.4-7.



Figure 4.4-7: Deflected shape of Specimen 3 after failure

The same pattern in terms of failure was seen in each specimen. For comparison, images showing the flexural cracking in the bottom of the deck and crushing in the top of the deck have been provided for each test specimen. Previously shown Figure 4.4-6 shows the concrete deck after failure for Specimen 1. The failure in the deck of Specimen 2 can be seen below in Figure 4.4-8. The failure of the concrete deck for Specimen 3 can also be seen below in Figure 4.4-9.

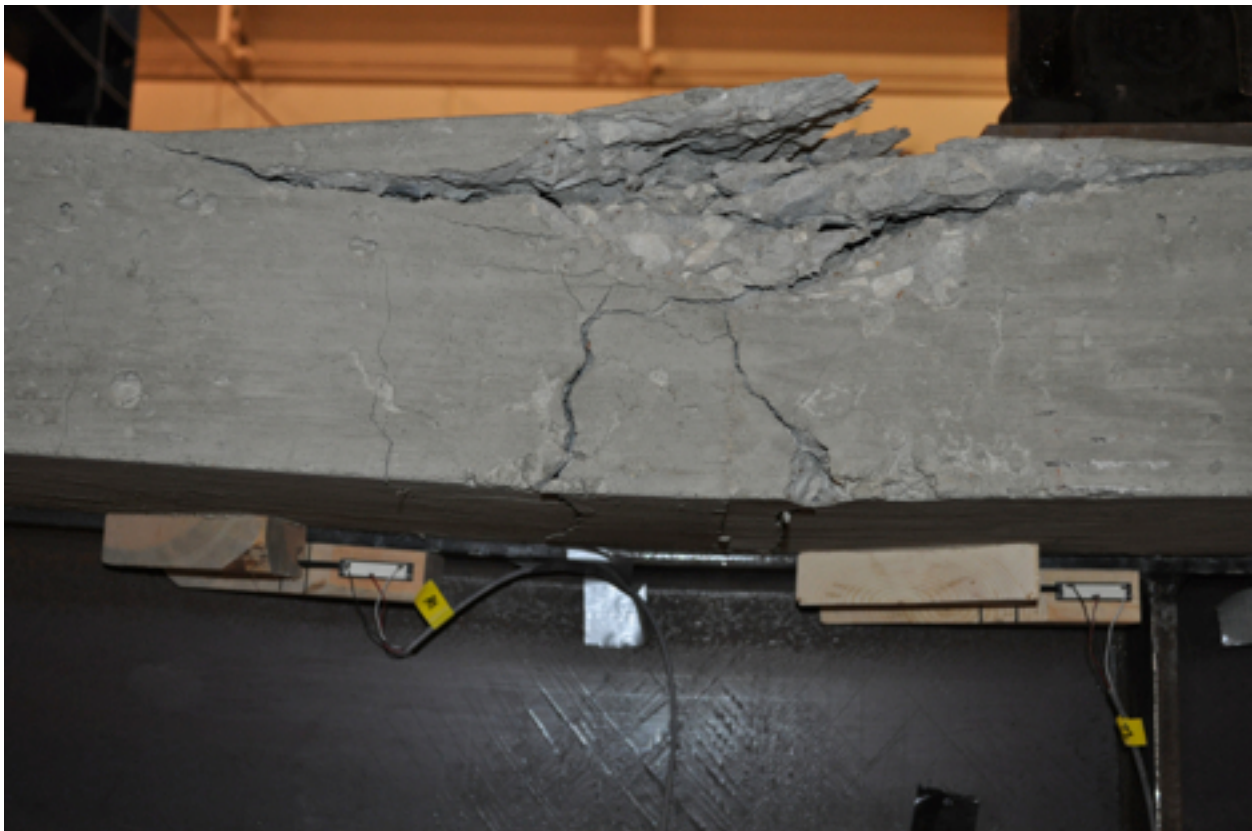


Figure 4.4-8: Concrete deck failure of Specimen 2



Figure 4.4-9: Concrete deck failure in Specimen 3

For Specimen 4, a close up image of the cracking of the bottom of the deck has been shown in Figure 4.4-10. A close up image of the crushing of the concrete on top of the deck is shown below in Figure 4.4-11. The onset and extent of deck cracking and crushing was essentially identical to that of Specimens 1 through 3. As Specimen 4 was not loaded as far beyond failure, the cracks and regions of crushed concrete are not as apparent in the previous specimens through photographs.



Figure 4.4-10: Cracking in bottom of deck for Specimen 4 after failure



Figure 4.4-11: Crushing of concrete deck for Specimen 4 after failure

Based on the observations of the researchers, as well as all photographs and recordings of testing, there is no clear evidence to indicate a difference in performance between beams achieving composite action using 1.25" large diameter studs and those achieving composite action using 7/8" diameter studs. Additionally, there is no meaningful observed evidence to indicate a difference in performance between specimens with uniform stud spacing and those with more widely spaced stud clusters.

4.5 Numerical Results and Analysis

Load Deflection Behavior

One of the key advantages of composite construction for bridges is improved load deflection behavior, meaning that a composite bridge would undergo less deflection under the same load when compared to a non-composite bridge. Therefore, this is an important point of comparison for performance among test specimens. Figure 4.5-1 shows a plot of the applied moment at midspan against the measured vertical deflection at midspan for each specimen. This graph clearly shows similar load deflection behavior between all of the specimens all the way until after the point of failure when the specimens began to undergo very large deflections. Even after failure, the trend among all of the beam specimens is quite similar with the exception of Specimen 4 where the full post-failure behavior of the beam was not able to be recorded.

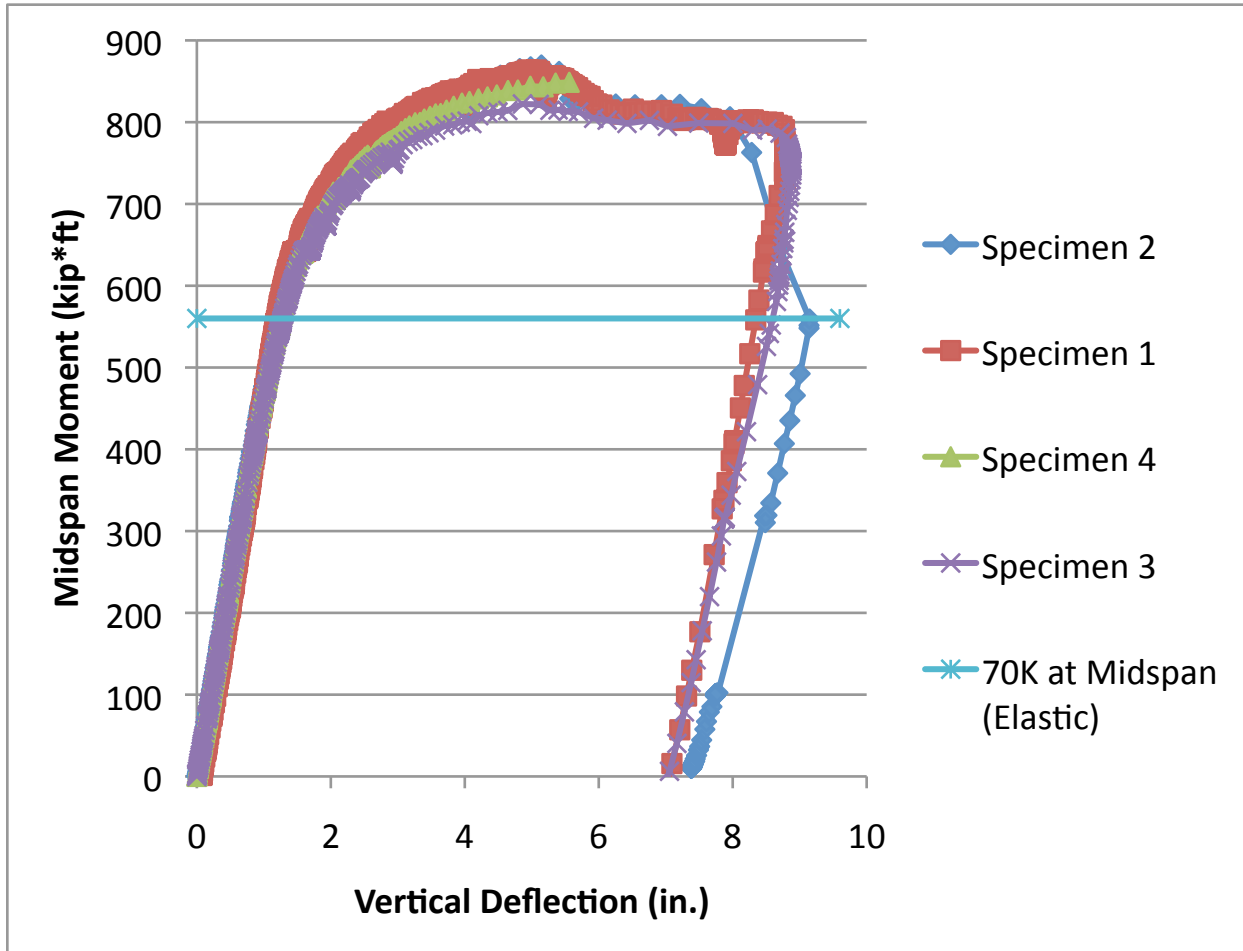


Figure 4.5-1: Plot of Midspan Moment vs. Midspan Vertical Deflection

Table 4.5-1 shows the deflections occurring with 70K at midspan and the beams behaving elastically. The deflections for Specimens 1 and 2 were nearly identical with less than 0.01" of difference. The deflection of Specimens 3 and 4 were also quite close, differing by less than 0.04". The deflections were higher when the studs were more widely spaced, however, this increase was still approximately 0.1".

Table 4.5-1: Midspan Deflections with 70K at Midspan (Elastic)

Specimen	1	2	3	4
Deflection with 70K at Midspan	1.200	1.207	1.301	1.263

Table 4.5-2 shows the deflection at midspan occurring at the peak applied Moment. Among specimens with uniform spacing, Specimen 2 with 1.25" diameter studs had nearly an inch less in total deflection. However between specimens with stud clusters, the 7/8" diameter stud specimen had nearly 0.7" less in deflection at midspan. Comparing between stud configurations, there was essentially no difference seen with 7/8" diameter stud specimens in terms of deflection between the uniform spacing configuration and clustered spacing configuration. For the 1.25" diameter stud specimens, there was an increase of nearly 1.5" of additional deflection in moving from the uniform spacing configuration to the clustered spacing configuration.

Table 4.5-2: Midspan Deflections Under Peak Applied Moment

Specimen	1	2	3	4
Deflection at Peak Moment (in)	4.941	3.96	4.863	5.560

This evidence suggests that for the uniform spacing configuration, the large diameter studs performed as well or better in terms of beam deflection. For the clustered spacing configuration, elastically, the specimens with large diameter studs clearly performed as well or better than the standard diameter studs. At peak moment, this was not the case, however it must be considered that these deflections were not taken at exactly the same moment values. When plotting the ratio of midspan moment to theoretical moment capacity against the midspan deflection, the load deflection trends for the specimens become even more tightly clustered as can be seen in Figure 4.5-2.

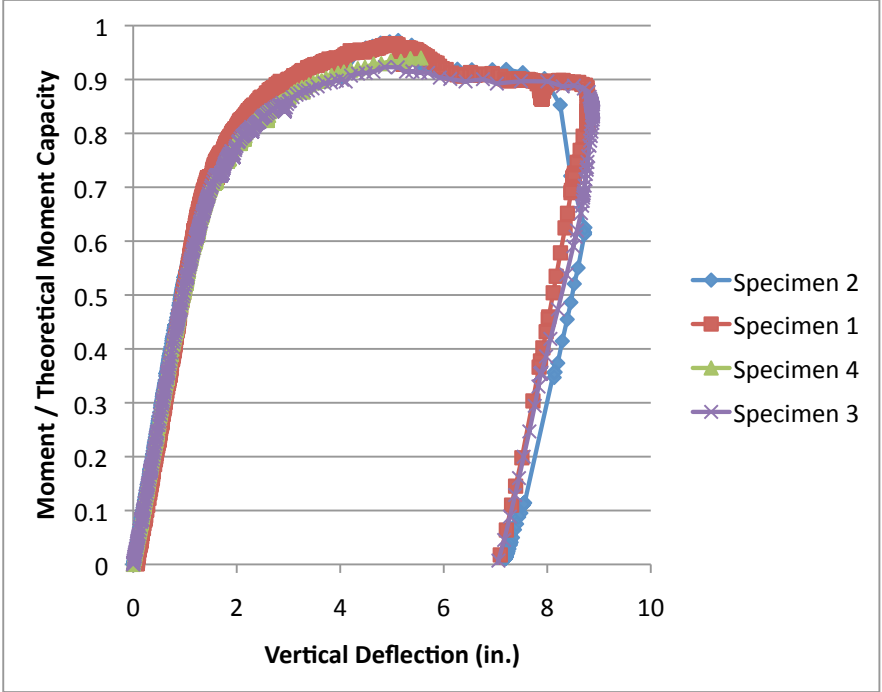


Figure 4.5-2: Plot of the Ratio of Applied Midspan Moment to Theoretical Moment Capacity vs. the Vertical Deflection at Midspan

Slip Behavior

Slip or relative longitudinal movement between the concrete deck and steel beam at their interface is an important indicator of the performance and behavior of the shear studs as they essentially provide the resistance to this movement. To capture this, laser type displacement sensors and piston type displacement sensors were used at the interface to capture this movement. Using this data, the slip has been quantified in several key ways.

First, cumulative slip will be examined. Cumulative slip is essentially the total movement of the slab relative to the steel section over the entire length of the beam. It was tabulated by taking the difference of the readings from the laser sensor positioned at one end of the specimen and the laser sensor positioned at the opposite end of the specimen. With the sign convention used, these readings carried opposite signs, so this operation was effectively the summation of the magnitudes of the two laser readings at the interface. A plot of the cumulative slip versus moment can be seen below in Figure 4.5-3. The cumulative slip is plotted against the moment normalized with the theoretical moment capacity in Figure 4.5-4. Table 4.5-3 lists the cumulative measured slab slip at the time of peak applied moment at midspan.

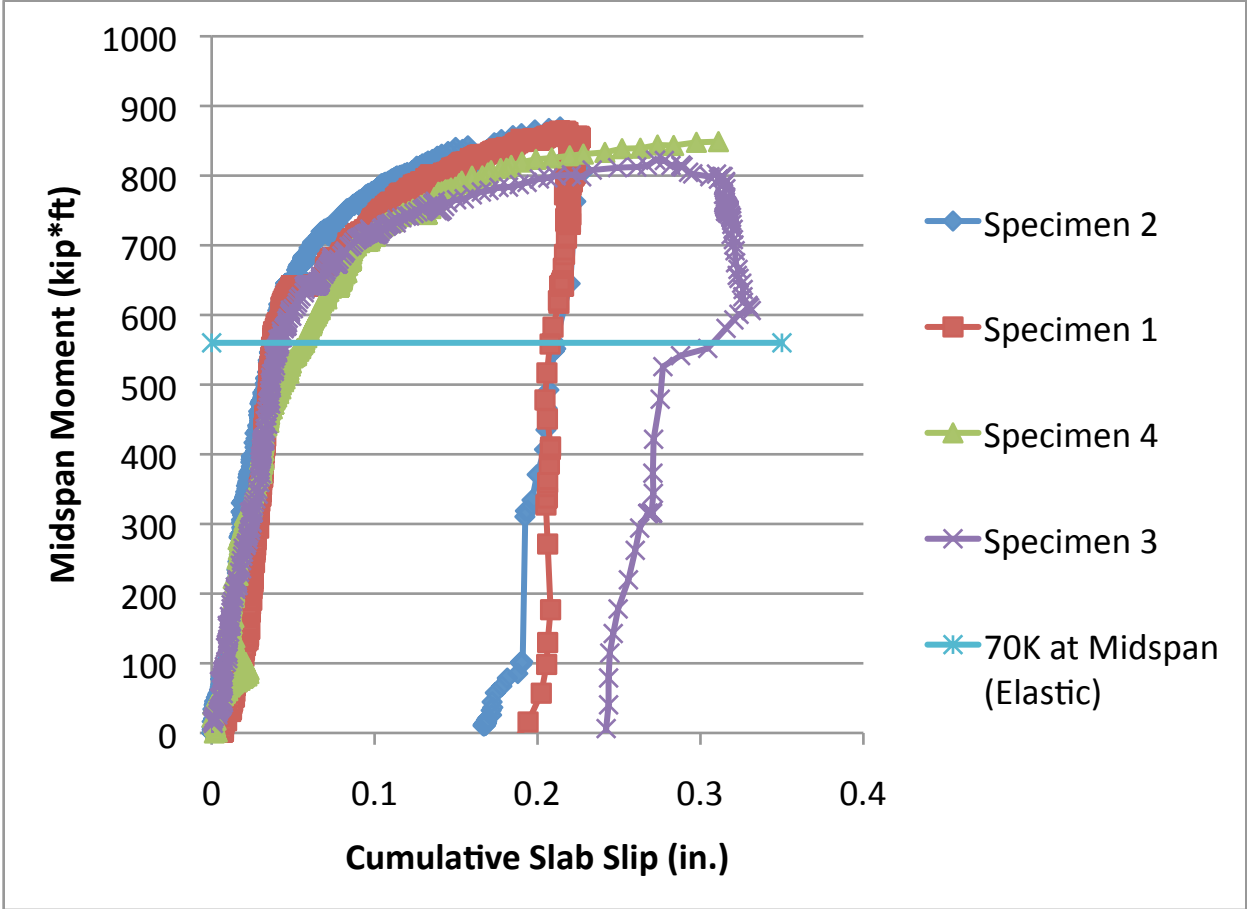


Figure 4.5-3: Plot of Midspan Moment vs. Cumulative Slab Slip

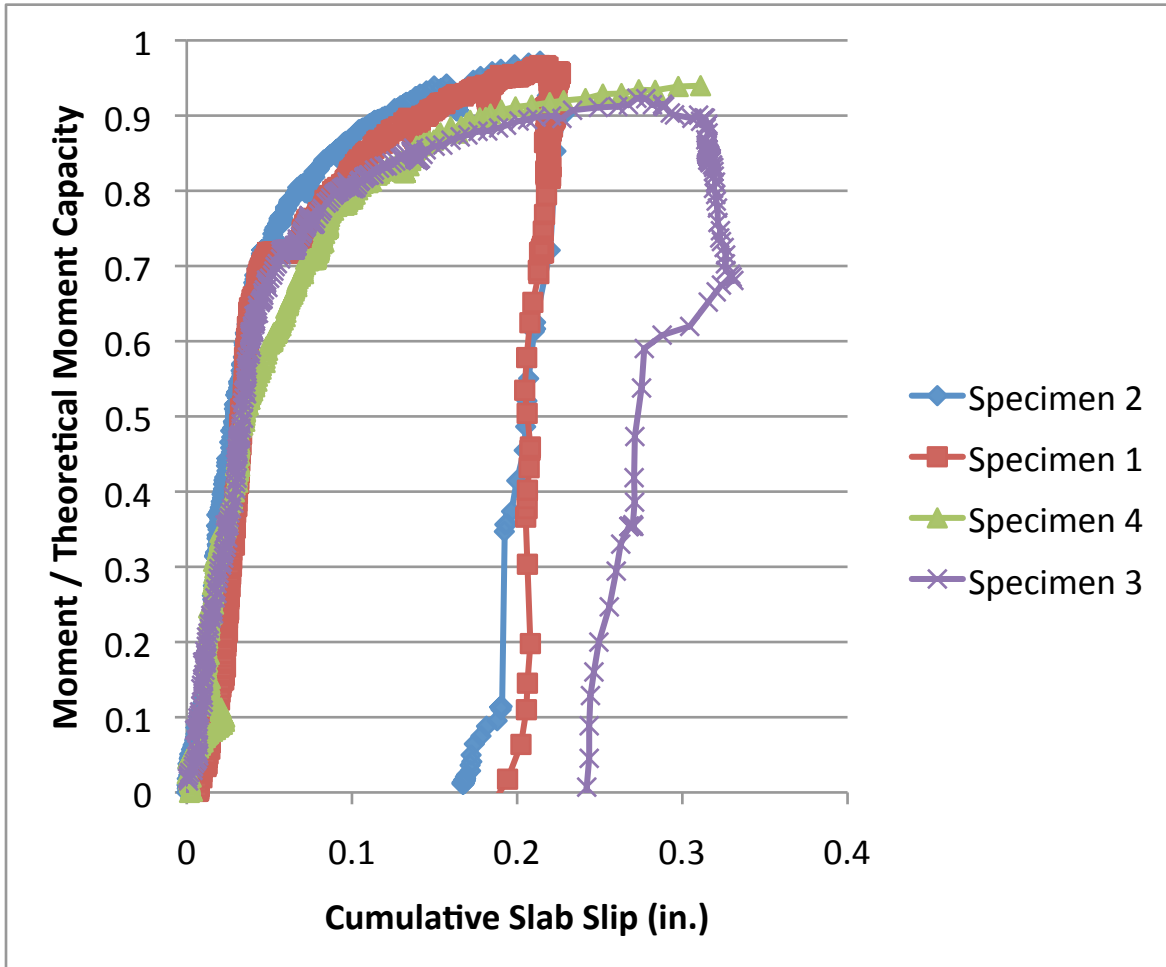


Figure 4.5-4: Plot of the Ratio of Moment to Theoretical Moment Capacity vs. Cumulative Slab Slip

Table 4.5-3: Cumulative Slip Values at Peak Applied Moment

Specimen	1	2	3	4
Cumulative Slip at Peak Moment (in)	0.214	0.157	0.272	0.311

The graphs shown in Figures 4.5-3 and 4.5-4 seem to indicate that within each pair of similarly configured specimens, the performance and general trend are quite similar with regard to slip behavior. Specimens 3 and 4 with the larger stud spacing with clusters show a trend of larger cumulative slips at the point of the peak moment. This is confirmed by Table 4.5-2 where it is seen that Specimen 1 had a lower cumulative slip than Specimen 3 while Specimen 2 also had lower cumulative slip than Specimen 4. It is noted that the magnitude of this increase was larger in the case of the large diameter studs. For the first pair of beams, Specimen 2 showed slightly lower slip. The trend was reversed for the second pair of beams where Specimen 3 showed a lower cumulative slip reading.

With piston type slip sensors placed along the length of the beam, the slip at various points along the length of the beam can be examined for each specimen. The readings of each individual sensor will be defined as the measured slip, which is simply the recorded piston displacement from that sensor at a particular time. The measured slip from each sensor is given below in Figures 4.5-5 and 4.5-6. Figure 4.5-5 shows the measured slip readings when 70 kips was applied through the actuator at midspan which has been selected as a point where Specimen behavior appeared to be fully elastic. Figure 4.5-6 shows the measured slip at the time of the peak applied moment.

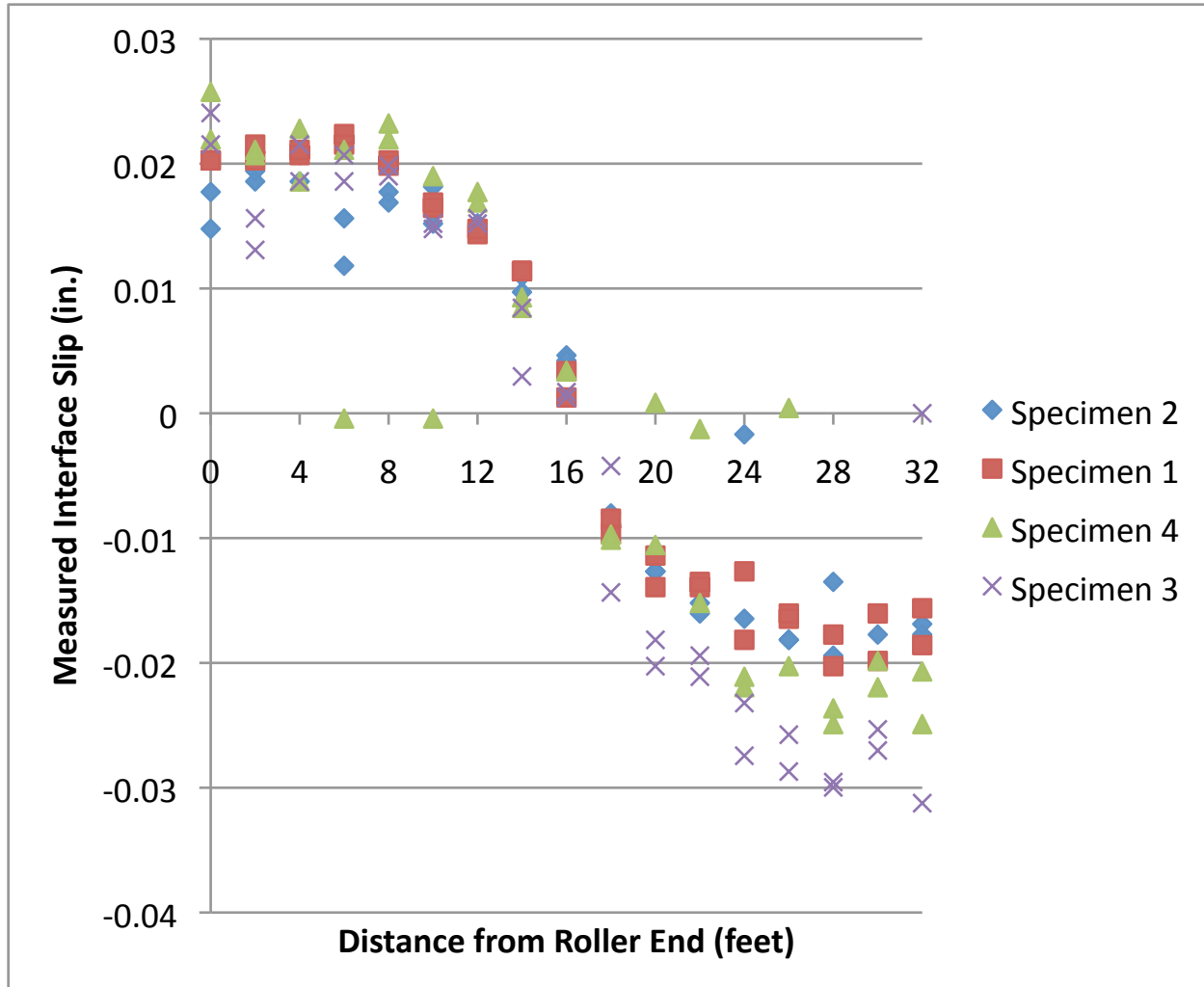


Figure 4.5-5: Plot of Measured Slip vs Distance Along the Beam with 70 K at Midspan and Elastic Behavior

In the elastic range, with 70 kips at midspan, the measured slip readings are very small. The data points are primarily clustered in two bands, one positive nearest the roller end and one negative band near the pinned end. This is expected as with 70 kips at midspan, there are

two bands of uniform shear. The data points line up fairly closely although in the negative band, Specimen 3 does exhibit slightly higher values than the other specimens. However, given that the difference is on the order of 1 hundredth of an inch, there is no reason to believe that this is a significant difference.

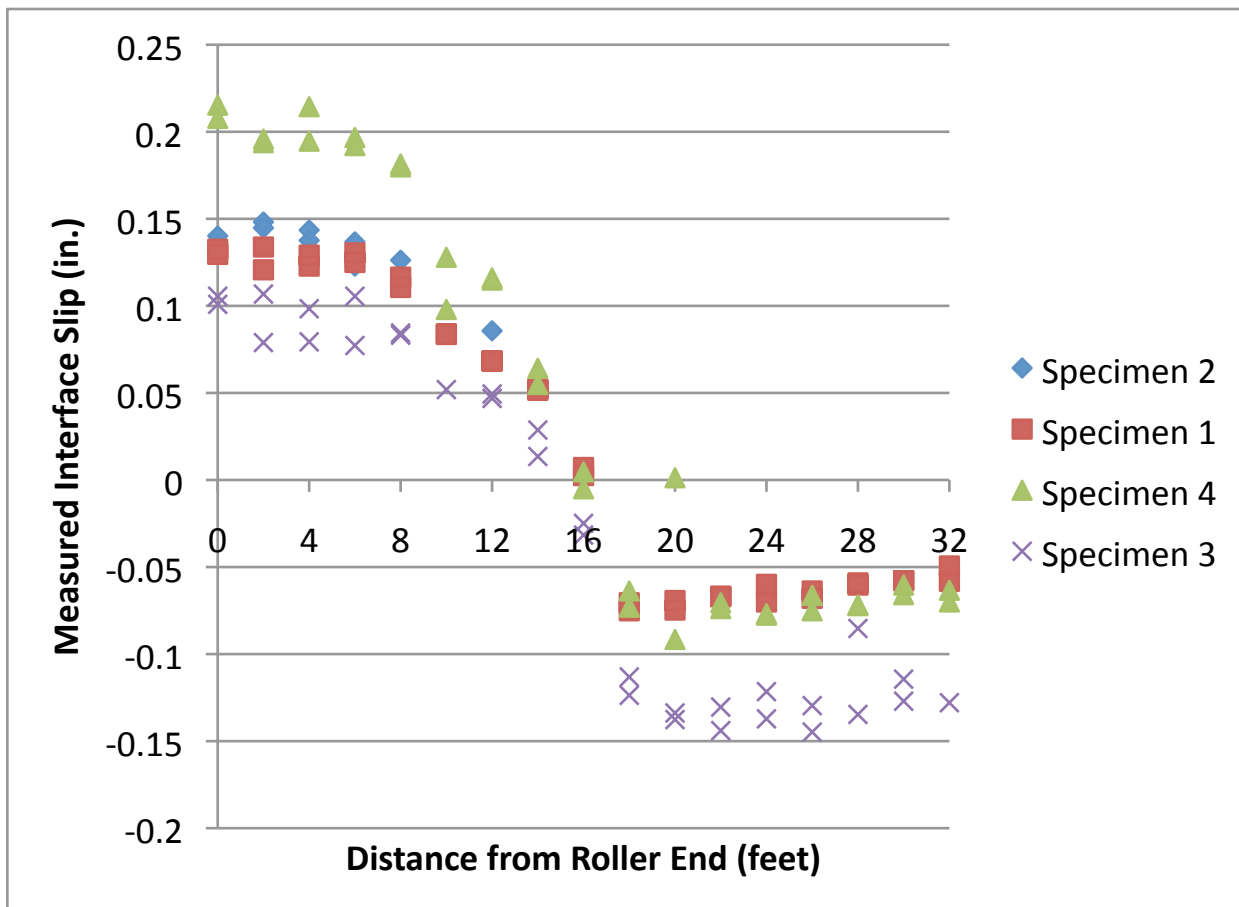


Figure 4.5-6: Plot of Measured Slip vs Distance Along the Beam at Peak Moment

The displayed trend is similar at the time of the peak applied moment as well except that the magnitudes of the measured slip readings have increased. There are essentially two bands, one positive near the roller end of the beam and one negative near the pinned end of the beam. The data points for Specimens 1 and 2 line up nearly on top of each other and there is no evidence to suggest a difference in measured slip readings along the length of the beam between the specimen with 1.25" studs and the specimen with 7/8" studs. Interestingly, the measured slip in Specimens 3 and 4 do not line up as well. They both show the same type of trend, however, Specimen 3 displays smaller measured slip readings in the positive band and higher magnitude measured slip readings in the negative band. In the negative band, Specimen 4 lines up very closely to Specimens 1 and 2, but in the positive band had higher measured slip readings. For Specimen 3, in the negative band it displayed higher magnitude slip readings while having slightly smaller slip readings in the positive band. There is no readily apparent explanation for these differences displayed in the second pair of test specimens. It should be noted that for each specimen the magnitude of the positive and negative bands differed. Given the loading configuration used, this would indicate that while not addressed by the current AASHTO (2010) code, that the load configuration and local shear and moment values may have an influence on the slip performance of shear studs.

Another type of slip measurement was computed using data from the piston type displacement sensors. This type of slip will be referred to as stud slip. The stud slip is essentially the difference in slip readings from a pair of slip sensors with one on each side of a stud or stud group. This measurement is intended to show how much slip is occurring at each

stud or stud group. To display this data, four plots were constructed and can be seen in Figures 4.5-7, 4.5-8, 4.5-9, and 4.5-10. Each data point on these plots was computed using input from four sensors. The reading from the sensor on one side of the beam immediately beyond the stud or stud group longitudinally was subtracted from the reading of the sensor immediately prior to the stud or stud group on the same side of the beam. The same value was then calculated for the pair of sensors on the opposite side of the beam. Each data point then represents the average of the difference in readings on each side. As Specimens 1 and 2 had different stud spacings from Specimens 3 and 4, the readings for each pair of beams have been plotted separately. The first pair of figures displays the stud slip readings against position when the beams were still behaving elastically with 70 kips at midspan. The second pair of figures shows the stud slip for the specimens when the peak applied moment occurred.

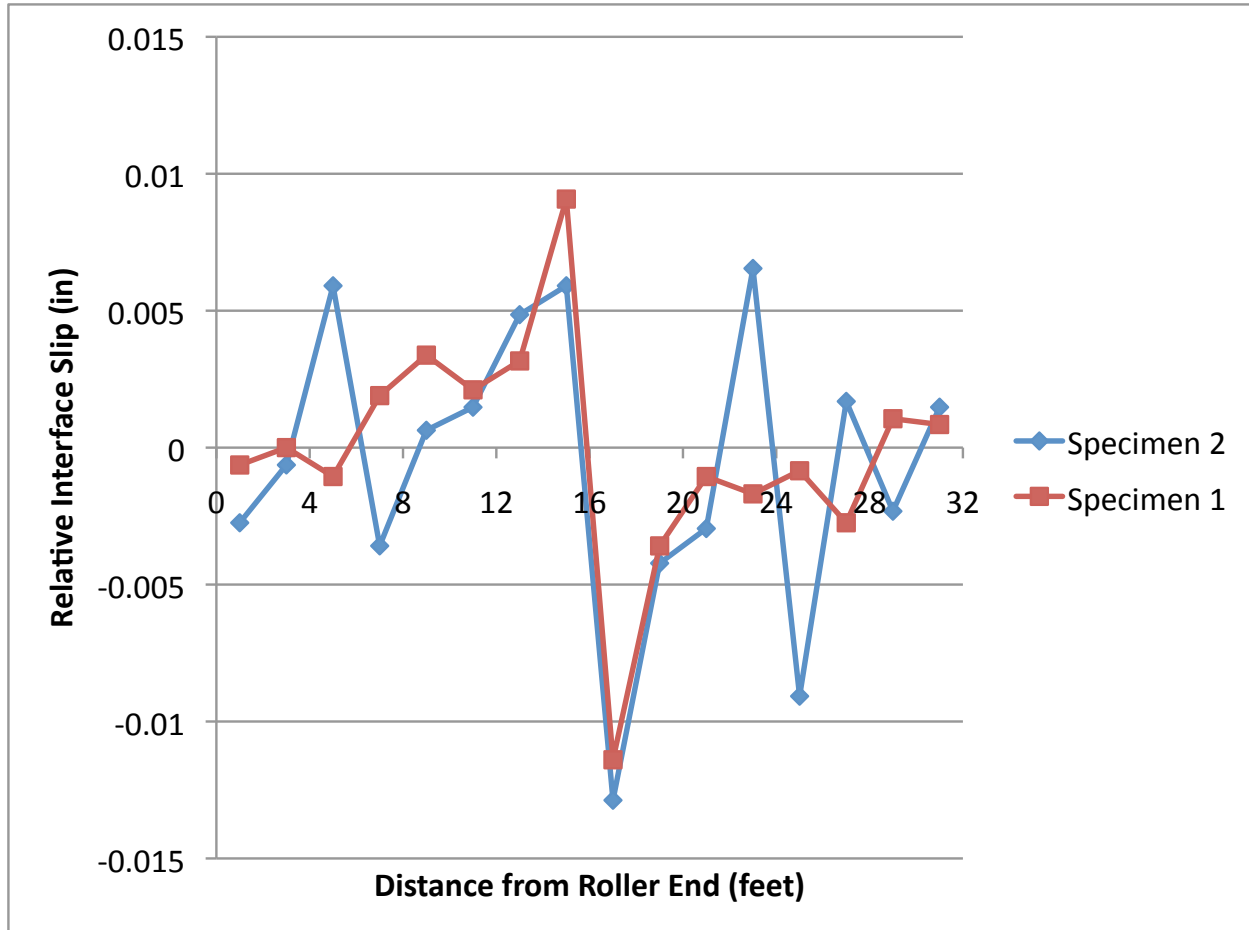


Figure 4.5-7: Plot of Stud Slip vs Distance Along Beam with 70 K at Midspan and Elastic Behavior for Specimens 1 and 2

In Figure 4.5-7, the stud slips are shown for Specimens 1 and 2 and several trends can be seen. Both specimens display large spikes for the readings at the stud locations on either side of the midspan load. Other spikes are visible and do differ more between the specimens, but are considerably smaller and given the small graph scale do not represent any significant

finding. The spike at either side of midspan is most likely due to the effect of the high concentrated load at midspan coupled with the higher moment in this region.



Figure 4.5-8: Plot of Stud Slip vs Distance Along Beam with 70 K at Midspan and Elastic Behavior for Specimens 3 and 4

Specimens 3 and 4 also show spikes in the stud pairs near the midspan load. This is likely due to the same reasons as for Specimens 1 and 2. Overall, the general pattern exhibited by these specimens is closer than the previous pair of specimens. It should be noted that the magnitude of the stud slips is higher, but the total number of stud groups is also reduced.

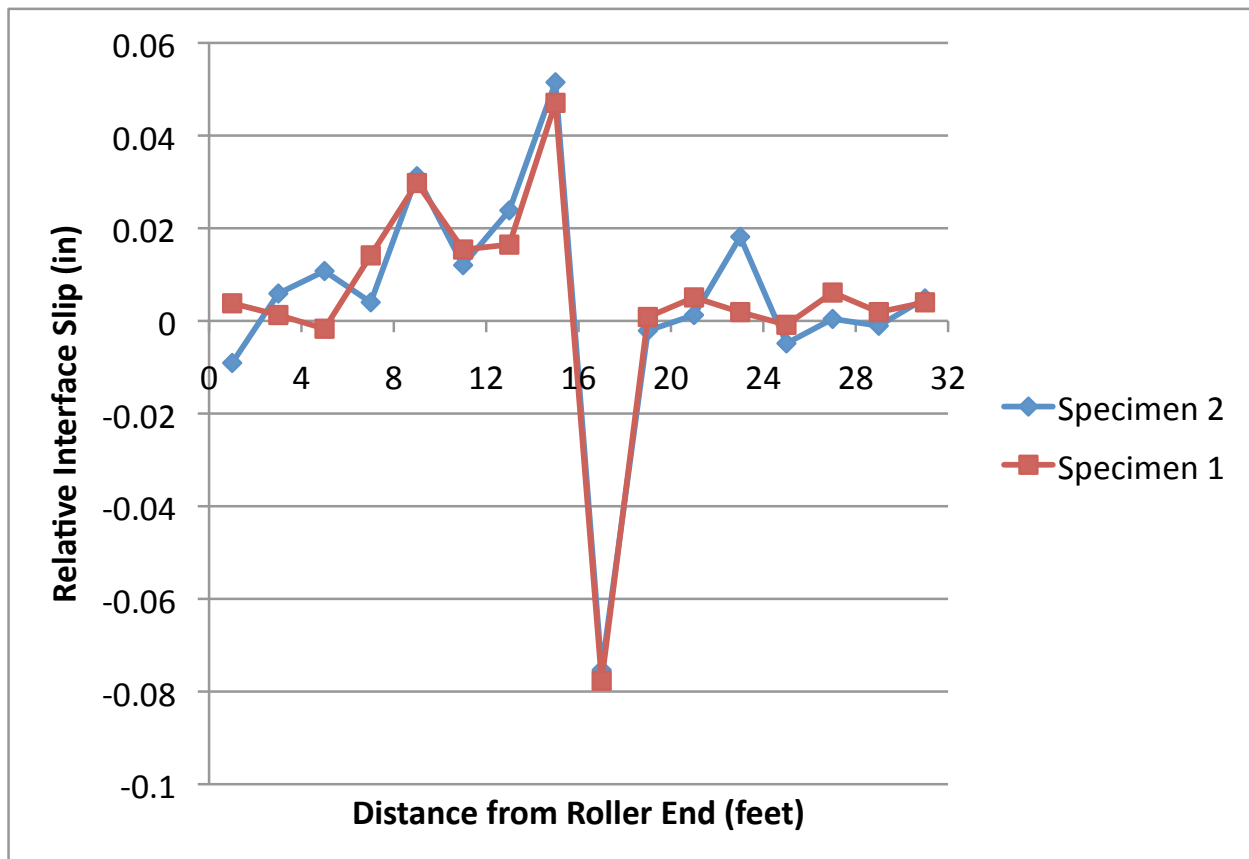


Figure 4.5-9: Plot of Stud Slip vs Distance Along Beam at Peak Applied Moment for Specimens 1

and 2

At peak load for Specimens 1 and 2, magnitudes of the stud slips have clearly increased since the plot shown with only 70 kips at midspan. The alignment of the values for the two specimens is also much closer. The same pattern with large peaks for stud slips to either side of the midspan load is still clearly visible. In this graph, there is also a much smaller quarterspan peak visible. Comparing the trend of stud slips between Specimens 1 and 2, there is no evidence to suggest that in terms of slip, there is a difference in performance between normal and large diameter shear studs.

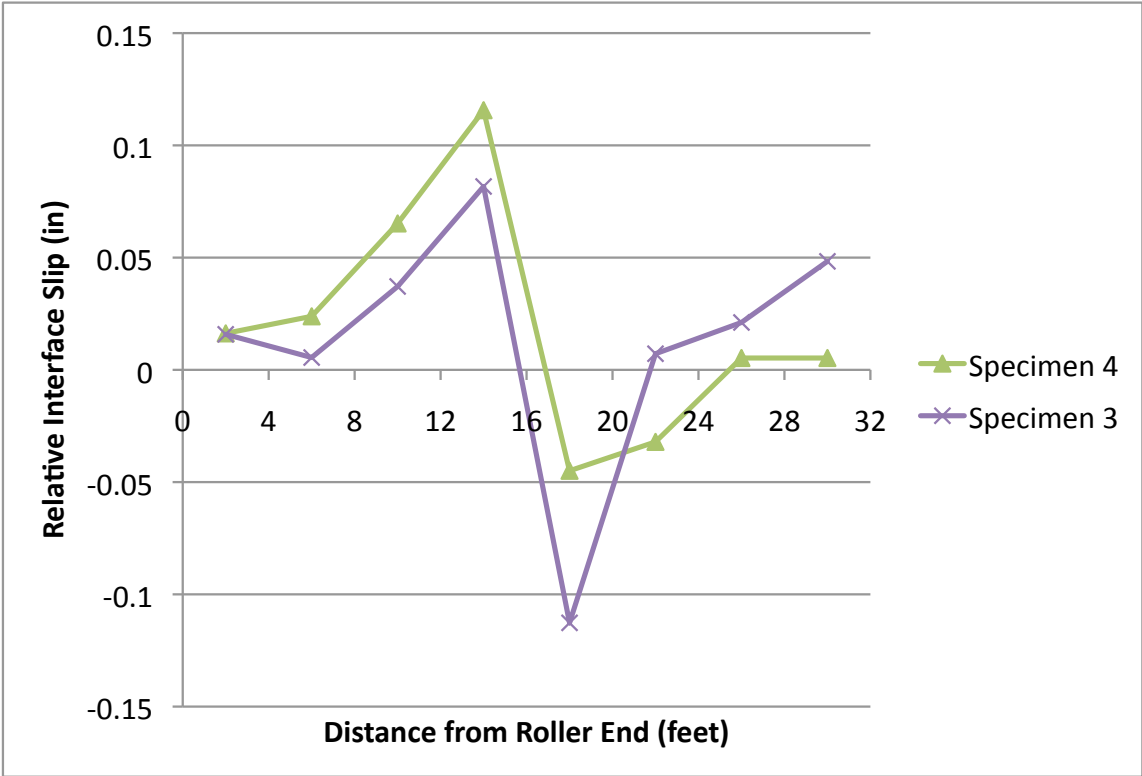


Figure 4.5-10: Plot of Stud Slip vs Distance Along Beam at Peak Applied Moment for Specimens 3 and 4

In Figure 4.5-10, Specimens 3 and 4 display a very similar pattern in terms of stud slip. As has been seen in all previous stud slip plots, there are large peaks to either side of the midspan load. There is not a clear peak displayed near the quarterspan load. The overall magnitude of the peaks is larger for Specimens 3 and 4 than for the first pair of specimens, which is again not unanticipated given that the the number of stud groups is reduced. The magnitude of the highest stud slip value near the midspan peaks is very similar between Specimens 3 and 4. Given this and the overall similar trend displayed in the data, it does not appear that there is a clear basis to suggest a difference in performance between the 1.25" diameter studs and the 7/8" diameter studs.

Strain Behavior

In addition to the sensors directly measuring slip at the concrete to steel interface, there were also strain gages on both the concrete and steel at this interface as well as other locations within the cross section to indicate any important strain differentials between the materials. As concrete strain gages could not be applied directly at the point of load application, the eighth span locations were instrumented with strain gages over the full height of the cross section. The 3/8th span strain profiles are given in Figures 4.5-11 and 4.5-12, first for when the specimen behavior appeared fully elastic with 70K at Midspan, and then when the specimens were under the peak applied moment.

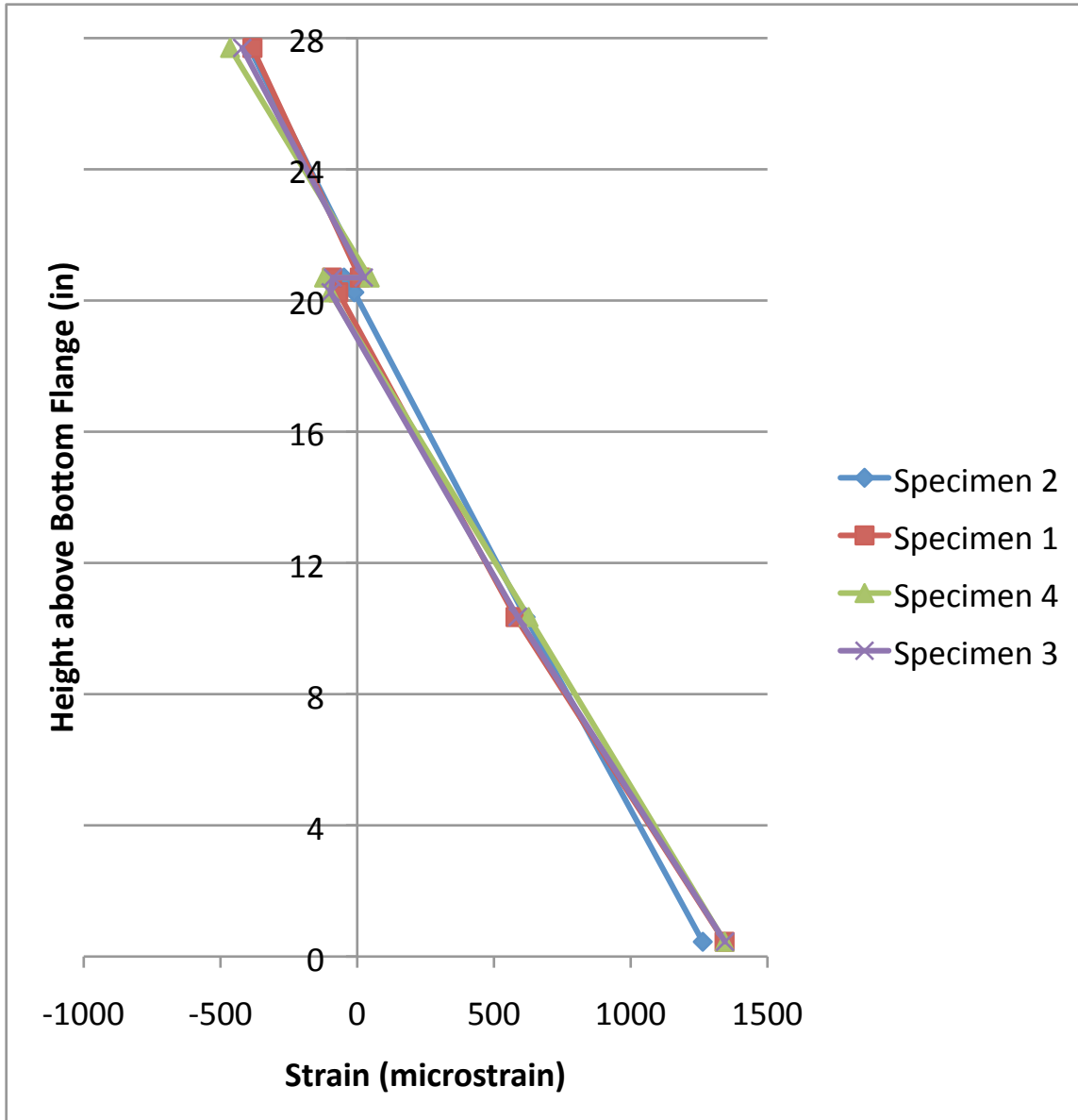


Figure 4.5-11: 3/8th span strain profile with 70 K at midspan

With 70K at midspan, the data points for all for specimens fall almost directly on top of each other for every data point. The strain profile appears very linear indicating elastic

behavior. The differential strain at the steel to concrete interface is very small. It may still be seen from this small difference however, that full composite behavior is not obtained in any of the specimens. There is no evidence provided by this data to suggest a difference in strain behavior between the normal diameter studs and large diameter studs or between the uniformly spaced studs and the widely spaced stud clusters within the elastic range.

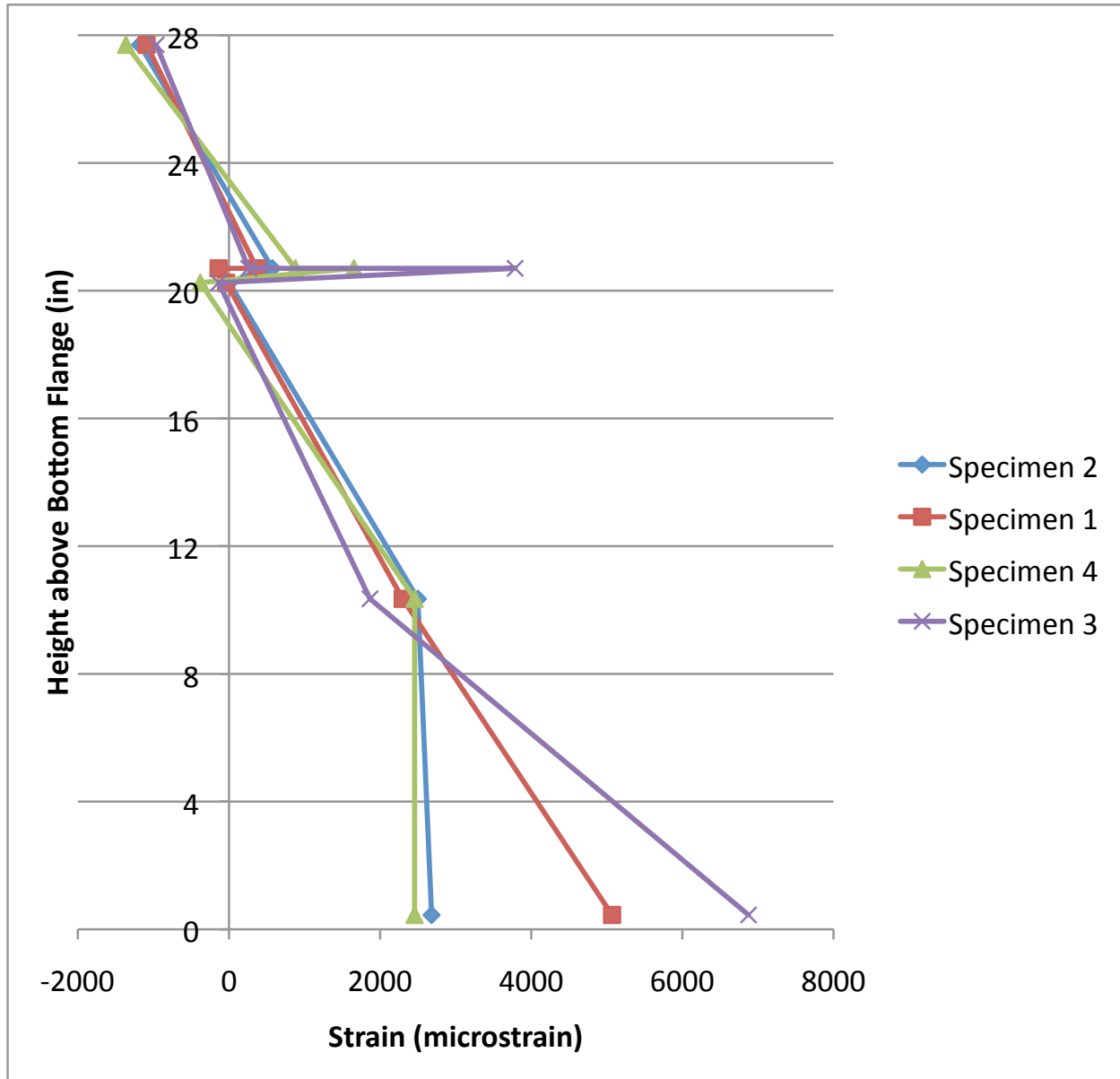


Figure 4.5-12: 3/8th span strain profile under peak applied moment at midspan

Under peak applied moment, the strain behavior is similar between the specimens, however, more differences are discernible. There are clearly kinks visible in the strain profiles

for each of the specimens indicating non-linear behavior. The strain differential at the steel to concrete interface is also much more visible. This is particularly evident for Specimen 3. There are two neutral axes clearly visible in this plot, one in the steel section and another in the concrete section indicating that full composite behavior is not seen in the specimens at this stage of the test. Both specimens with large diameter studs display lower bottom flange strains, though there is no clear explanation offered for this. Specimens 3 and 4 do both display larger steel strains at the steel to concrete interface which is also indicated by the larger slip measurements recorded for these specimens. Aside from that, there is little else to indicate a difference in strain behavior between the uniform and clustered spacing configurations. There is also no clear evidence indicating a difference in strain behavior between the 7/8" diameter shear studs and 1.25" diameter shear studs within each pair of specimens.

Chapter 5: Conclusions and Recommendations

5.1 Overview

Chapter 5 begins by providing a summary of the key findings and conclusions of the research effort. After summarizing the findings, recommendations for incorporating the results of this experimental effort into future updates to AASHTO (2010) are provided. Finally, recommendations for future research and advancement of the knowledge base on the implementation of large diameter shear studs in composite bridge construction will be discussed.

5.2 Conclusions

Several key findings can be drawn from this effort regarding 1.25" large diameter shear studs in composite bridge construction:

- A partial composite action analysis revealed that specimens fabricated with large diameter shear studs were able to gain the same or higher percentages of theoretical strength capacity when spaced uniformly or in widely spaced clusters as compared to standard diameter studs in comparable configurations.
- Strength performance of specimens with widely spaced stud clusters was slightly reduced compared to specimens with uniform stud spacing regardless of stud diameter.

- Welding of large diameter studs with commercially available stud welding equipment is feasible and appears to produce consistent, high quality welds.
- The visually observed specimen behavior and failure mechanisms were consistent between all specimens regardless of stud type or spacing pattern utilized.
- Differences in slip behavior between each pair of similarly configured test specimens were minimal, however, the pair of specimens with larger, clustered spacing exhibited higher cumulative slip than the uniformly spaced specimens.
- Elastic strain profiles for all specimens were nearly identical.

In examining the body of evidence produced, there is considerable evidence to suggest that large 1.25" studs exhibit similar or greater strength and ductility when utilized in composite bridge construction as compared to normal 7/8" diameter studs. There is little evidence to suggest otherwise. In the uniform studs spacing configuration in terms of specimen slip, strain behavior, and deflection, the large diameter studs also exhibited performance meeting or exceeding those of normal diameter specimens. The evidence indicates that the specimens with widely spaced, clustered configurations did not perform as well in terms of strength, slip, or deflection. The large diameter stud specimen in this configuration exhibited similar behavior to the specimen with standard diameter studs. The decrease in strength in moving from large diameter studs at uniform spacing to those more widely spaced and arranged in pairs was less than the corresponding drop in strength seen in normal diameter studs. This trend was

reversed however, for slip where the large diameter studs showed a greater decrease in performance than the normal diameter studs.

5.3 Design Code Recommendations

This research effort has not revealed any concerns with the strength performance of large diameter studs. There is also no evidence to suggest a fundamental difference in the ductile behavior and load redistribution abilities of large diameter studs as compared to conventionally sized studs used in composite bridge construction. It is, therefore, concluded that highway bridges utilizing large 1.25" diameter studs may be safely designed for the strength limit state using the applicable strength provisions of AASHTO (2010) without modification. Utilizing this design procedure, it appears the effective factor of safety for large diameter studs would be equal to or greater than that for designs utilizing conventional studs sizes.

5.4 Future Research Recommendations

With previously performed push out testing performed by other researchers and the results of flexural testing conducted as part of this research, there is a clear body of evidence suggesting that the strength provisions of current design codes are adequate for designing large diameter shear studs. Previously performed research at Auburn University by Mundie (2011) has indicated that current fatigue provisions of various design codes also appear adequate for fatigue limit state design of large diameter shear studs. With those key elements established,

additional testing on serviceability limit states, particularly for unusual or widely spaced stud spacing patterns as might be used in precast deck panels with discrete pockets of shear studs may be warranted, as there did appear to be some indications of increasing deflections and slip seen in specimens with large diameter studs grouped at a wider spacing.

Fabricating a full scale composite highway bridge using large diameter shear studs would provide further insight into the practical benefit and possible time savings of using large diameter studs. Additionally, in the future being able to instrument a structure such as this would further validate the complete performance of the bridge and its shear connectors for all limit states.

References

AASHTO (2010). *AASHTO LRFD Bridge Design Specifications*, 5th Edition. Washington D.C.

AISC (2010). *Specification for Structural Steel Buildings*. Chicago.

Badie, Sameh S., Tadros, Maher K., Kakish, Hussam F., Spittgerber, Darin L., Baishya, Mantu C., (2002). *Large Shear Studs for Composite Action in Steel Bridge Girders*. *Journal of Bridge Engineering*, May/June 2002.

Lee, Pil-Goo., Shim, Chang-Su., and Chang, Sung-Pil. (2005). *Static and Fatigue Behavior of Large Stud Shear Connectors for Steel-Concrete Composite Bridges*. *Journal of Constructional Steel Research* 61. p 1270-1285.

Mundie, Daniel L. (2011). *Fatigue Testing and Design of Large Diameter Shear Studs Used in Highway Bridges*. M.S. Thesis. Auburn University.

Slutter, Roger G. and Driscoll, George C. (1965). *Flexural Strength of Steel Concrete Composite Beams*. *Journal of the Structural Division, ASCE* Vol. 91 No. ST2.

Shim, Chang-Su., Lee, Pil-Goo., and Yoon, Tae-Yang. (2004). *Static Behavior of Large Stud Shear Connectors*. Engineering Structures 26. p 1853-1860.

A1.2 7/8" Diameter Shear Stud Mill Test Report



2211 Century Center Boulevard
 Irving, TX 75062
 Tel: 972.721.9055 • Fax: 972.438.7883
 800.635.9353
 Web: www.nelsonstudwelding.com

8/11/11 Certificate of Compliance

AUBURN UNIVERSITY
 CIVIL ENGINEERING CENTER
 238 HARBERT ENGINEERING CENTER
 AUBURN UNIVERSITY

AL 36849

Material Description	Quantity	Heat Number	Lab Number
S3L 7/8 X 5 3/16 MS	120	10129960	18355

Nelson Order Number: 219301 Customer P.O.: CREDIT CARD

The product supplied under the contract or purchase order number shown is certified to comply with the latest revision of one or more of the applicable product specifications therein; AWS D1.1, AWS D1.5, AWS D1.6, ISO 13918, BS 5950, ASTM A108-07, ASTM A29, ASTM A276, ASTM A493, ASTM A496-07, ASTM A479, and ASTM A1022.

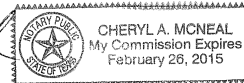
The chemical analysis reported below was extracted from the certified mill test report. This report will be supplied when specified in the customer order or upon request. The physical properties reported were determined to be in conformance using ASTM A370 testing procedure.

Nelson Stud Welding is an ISO/TS 16949:2009 certified supplier. Our IATF certificate # is 0091173. This material is free from mercury contamination and is RoHS compliant. This product is melted and manufactured in the USA. No weld repair was performed on the raw material or the studs.

Grade	C-1015
Heat Number	10129960
Ultimate PSI	65,800
Yield PSI	52,000
% Reduction of Area	59.0
% Elong. (in 2"or4D)	32.0
% Elong. (in 5D)	28.000
Carbon	.150
Manganese	.540
Phosphorous	.007
Sulphur	.008

I hereby certify that the data listed in this Certificate of Compliance is true and correct as contained in the company test records and that it complies with the specifications shown.

Authorized by:





CHARTER STEEL

A Division of
Charter Manufacturing Company, Inc.

LOAD

CHARTER STEEL TEST REPORT Reverse Has Text And Codes

1658 Cold Springs Road
Saukville, Wisconsin 53080
(262) 268-2400
1-800-437-8789
FAX (262) 268-2570

Nelson Stud Welding
7900 West Ridge Road
QC Department
Elyria, OH-44036
Kind Attn : QC Department

6/10

Cust P.O.	178119
Customer Part #	103004096
Charter Sales Order	10042231
Heat #	10129960
Ship Lot #	1038907
Grade	1015 M SK FG RHQ 57/64
Process	HR
Finish Size	57/64

I hereby certify that the material described herein has been manufactured in accordance with the specifications and standards listed below and on the reverse side, and that it satisfies these requirements.

Lab Code: 7388

Test Results of Heat Lot# 10129960

CHEM	C	MN	P	S	SI	NI	CR	MO	CU	SN	V
%Wt	.15	.54	.007	.008	.17	.04	.05	.01	.08	.005	.001
	AL	N	B	TI	CA	NB	SB	AS	PB		
	.023	.0070	.0001	.001	.0004	.001	.001	.002	.002		

JOMINY(HRC) JOM01
41

T.H. 6/22/11

JOMINY SAMPLE TYPE ENGLISH = C
CHEM. DEVIATION EXT.-GREEN =

Test Results of Rolling Lot# 1038907

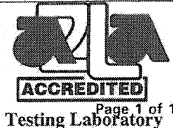
ROCKWELL B	# of Tests	Min Value	Max Value	Mean Value	RB LAB = 0358-02
REDUCTION RATIO = 49:1	3	65	67	66	

Specifications: Manufactured per Charter Steel Quality Manual Rev 9,08-01-09
Meets customer specifications with any applicable Charter Steel exceptions for the following customer documents:
Customer Document = MPS-102C Revision = E Dated = 28-MAY-02

Additional Comments: This material meets the chemistry requirements of ASTM-A108 (1999), EN 10025-2 S-235-J2G3 and the latest revision of ASTM A29.

LAB 18355

Charter Steel
Saukville, WI, USA



Rem: Load1, Fax0, Mail0

This MTR supersedes all previously dated MTRs for this order
Janice Barnard
Janice Barnard
Manager of Quality Assurance
06/08/2011

The following statements are applicable to the material described on the front of this Test Report:

1. Except as noted, the steel supplied for this order was melted, rolled, and processed in the United States meeting DFAR's compliance.
2. Mercury was not used during the manufacture of this product, nor was the steel contaminated with mercury during processing.
3. Unless directed by the customer, there are no welds in any of the coils produced for this order.
4. The laboratory that generated the analytical or test results can be identified by the following key:

Certificate Number	Lab Code	Laboratory		Address
0358-01	7388	CSSM	Charter Steel Melting Division	1653 Cold Springs Road, Saukville, WI 53080
0358-02	8171	CSSR/CSSP	Charter Steel Rolling/Processing Division	1658 Cold Springs Road, Saukville, WI 53080
0358-03	123633	CSFP	Charter Steel Ohio Processing Division	6255 US Highway 23, Risingsun, OH 43457
0358-04	125544	CSCM/CSCR	Charter Steel Cleveland	4300 E. 49th St., Cuyahoga Heights, OH 44125-1004
*	*	--	Subcontracted test performed by laboratory not in Charter Steel system	

5. When run by a Charter Steel laboratory, the following tests were performed according to the latest revisions of the specifications listed below, as noted in the Charter Steel Laboratory Quality Manual:

Test	Specification	CSSM	CSSR/CSSP	CSFP	CSCM/CSCR
Chemistry Analysis	ASTM E415; ASTM E1019	X			X
Macroetch	ASTM E381	X			X
Hardenability (Jominy)	ASTM A255; SAE J406; JIS G0561	X			X
Grain Size	ASTM E112	X	X	X	X
Tensile Test	ASTM E8; ASTM A370		X	X	X
Rockwell Hardness	ASTM E18; ASTM A370	X	X	X	X
Microstructure (spheroidization)	ASTM A892		X	X	
Inclusion Content (Methods A, E)	ASTM E45		X		X
Decarburization	ASTM E1077		X	X	X

Charter Steel has been accredited to perform all of the above tests by the American Association for Laboratory Accreditation (A2LA). These accreditations expire 01/31/13.

All other test results associated with a Charter Steel laboratory that appear on the front of this report, if any, were performed according to documented procedures developed by Charter Steel and are not accredited by A2LA.

6. The test results on the front of this report are the true values measured on the samples taken from the production lot. They do not apply to any other sample.
7. This test report cannot be reproduced or distributed except in full without the written permission of Charter Steel. The primary customer whose name and address appear on the front of this form may reproduce this test report subject to the following restrictions:
 - It may be distributed only to their customers
 - Both sides of all pages must be reproduced in full
8. This certification is given subject to the terms and conditions of sale provided in Charter Steel's acknowledgement (designated by our Sales Order number) to the customer's purchase order. Both order numbers appear on the front page of this Report.
9. Where the customer has provided a specification, the results on the front of this test report conform to that specification unless otherwise noted on this test report.





P.O. Box 398
110 Hopkins Street
Buffalo NY 14240

CERTIFICATION

CERTIFICATE	Rev
B104340	1
DATE	02/01/11
PAGE	12

S ALRO STEEL, AKRON H 4787 STATE RD I AKRON-CLEVELAND RD P CUYAHOGA FALLS OH 44223 T USA O	PURCHASE ORDER AK7682587 ORDER 691789-1 CUSTOMER ITEM 00203600 GRADE 1018 SIZE 1 1/4 LENGTH 11' 0" / 12' 6"	ITEM 111250132181 SHAPE Round SIZE MM 31.7500 MM LENGTH MM 3352.8 / 3810
---	--	---

ASTM A108 & A29 Spec/Rev: Spec/Rev: ASTM A108-07 Spec/Rev: ASTM A29-05

HEAT	GRAIN PRACTICE	SOURCE / MELTED	CAST	REDUCTION RATIO	DI
C83374_01	COARSE	ARCELORMITTAL-CANADA	STRAND	22.4:1	

CHEMISTRY											
C	MN	P	S	SI	NI	CR	MO	CU	AL	Y	
0.17	0.74	.016	.028	0.230	0.04	0.03	.007	.150	.001	.002	
N	TE	AS	PB	SE	BI	B	NB				
.004	N/A	N/A	N/A	N/A	N/A	N/A	.0002	.0010			

LOT	JOB	WEIGHT (LBS)	PIECES	LOT	JOB	WEIGHT (LBS)	PIECES
3512158	BS10840	4,044	80				

M.P. 8/10/11



WE, hereby certify that these goods were produced in compliance with all applicable requirements of sections 6, 7, and 12 of the Fair Labor Standards Act, as amended, and all regulations and orders of the United States Department of Labor issued under section 14 thereof. Material was not exposed to mercury or any metal alloy that is liquid at ambient temperature during processing or while in our possession. No weld repairs performed on the above material.

CERTIFICATE OF TEST

By: *Walter P. Kretzler*

Walter P. Kretzler - Director of Q.A./Chief Metallurgist

*lab
18432*

A1.3 1.25" Diameter Shear Stud Mill Test Report



2211 Century Center Boulevard
 Irving, TX 75062
 Tel: 972.721.9055 • Fax: 972.438.7883
 800.635.9353
 Web: www.nelsonstudwelding.com

9/30/11 Certificate of Compliance

AUBURN UNIVERSITY
 CIVIL ENGINEERING CENTER
 238 HARBERT ENGINEERING CENTER
 AUBURN UNIVERSITY AL

36849

Material Description	Quantity	Heat Number	Lab Number
S3L 1 1/4 X 5 1/4 MS	50	C83374-01	18432

Nelson Order Number: 219301

Customer P.O.: CREDIT CARD

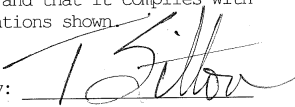
The product supplied under the contract or purchase order number shown is certified to comply with the latest revision of one or more of the applicable product specifications therein; AWS D1.1, AWS D1.5, AWS D1.6, ISO 13918, BS 5950, ASTM A108-07, ASTM A29, ASTM A276-04, ASTM A493, ASTM A496, ASTM A479, and ASTM A1022.

The chemical analysis reported below was extracted from the certified mill test report. This report will be supplied when specified in the customer order or upon request. The physical properties reported were determined to be in conformance using ASTM A370 testing procedure.

Nelson Stud Welding is an ISO/TS 16949:2009 certified supplier. Our IATF certificate # is 0091173. This material is free from mercury contamination and is RoHS compliant. No weld repair was made on the material or the studs.

Grade	C-1018
Heat Number	C83374-01
Ultimate PSI	85,000
Yield PSI	77,000
% Reduction of Area	57.0
% Elong. (in 2"or4D)	20.0
Carbon	.170
Manganese	.740
Phosphorous	.016
Sulphur	.028

I hereby certify that the data listed in this Certificate of Compliance is true and correct as contained in the company test records and that it complies with the specifications shown.

Authorized by: 



NIAGARA LASALLE CORPORATION
 P.O. Box 399
 110 Hopkins Street
 Buffalo NY 14240

CERTIFICATION

CERTIFICATE	Rev
B104340	1
DATE	02/01/11
PAGE	12

S H I P T O	ALRO STEEL, AKRON	PURCHASE ORDER	AK7682587	
	4787 STATE RD	ORDER	691789-1	
	AKRON-CLEVELAND RD	CUSTOMER ITEM	00203600	
	CUYAHOGA FALLS OH 44223	ITEM	111250132181	
	USA	GRADE	1018	
	SHAPE	Round		
	SIZE	1 1/4	SIZE MM	31.7500 MM
	LENGTH	11' 0" / 12' 6"	LENGTH MM	3352.8 / 3810

ASTM A108 & A29 Spec/Rev: Spec/Rev: ASTM A108-07 Spec/Rev: ASTM A29-05

HEAT	GRAIN PRACTICE	SOURCE / MELTED	GAST	REDUCTION RATIO	DI
C83374_01	COARSE	ARCELORMITTAL-CANADA	STRAND	22.4:1	

CHEMISTRY										
C	MN	P	S	SI	NI	GR	MO	CU	AL	V
0.17	0.74	.016	.028	0.230	0.04	0.03	.007	.150	.001	.002
N	TE	AS	PB	SE	BI	B	NB			
.004	N/A	N/A	N/A	N/A	N/A	.0002	.0010			

LOT	JOB	WEIGHT (LBS)	PIECES	LOT	JOB	WEIGHT (LBS)	PIECES
3512159	BS10840	4,044	80				

M.P. 8/10/11



WE, hereby certify that these goods were produced in compliance with all applicable requirements of sections 6, 7, and 12 of the Fair Labor Standards Act, as amended, and all regulations and orders of the United States Department of Labor issued under section 14 thereof. Material was not exposed to mercury or any metal alloy that is liquid at ambient temperature during processing or while in our possession. No weld repairs performed on the above material.

CERTIFICATE OF TEST By: *Walter P. Kretzler* Walter P. Kretzler - Director of Q.A./Chief Metallurgist

*lab
18432*

A1.4 Rebar Mill Test Report



CMC STEEL SOUTH CAROLINA
310 New State Road
Cayce SC 29033-3704

CERTIFIED MILL TEST REPORT
For additional copies call
800-637-3227

We hereby certify that the test results presented here are accurate and conform to the reported grade specification

Richard S. Ray
Richard S. Ray - CMC Steel SC

Quality Assurance Manager

HEAT NO.:2013157 SECTION: REBAR 13MM (#4) 60"0" 420/60 GRADE: ASTM A615-09b Gr 420/60 ROLL DATE: 03/11/2011 MELT DATE: 03/05/2011	S O L D T O	Sabel Steel Service Inc 749 N Court St Montgomery AL US 36104-2301 3342656771 3342643692	S H I P T O	Sabel Steel Service Inc 749 N Court St Montgomery AL US 36104-2301 3342656771 3342643692	Delivery#: 80470526 BOL#: 70165741 CUST PO#: 06-111-385E CUST P/N: DLVRY LBS / HEAT: 34628.000 LB DLVRY PCS / HEAT: 864 EA
--	----------------------------	---	----------------------------	---	---

Characteristic	Value	Characteristic	Value	Characteristic	Value
C	0.44%	Elongation test 1	12%		
Mn	0.73%	Elongation Gage Lgth test 1	8IN		
P	0.014%	Bend Test Diameter	1.750IN		
S	0.029%	Bend Test	Passed		
Si	0.20%	Pounds per Foot	0.642LB/FT		
Cu	0.16%	Rebar Deformation Avg. Spaci	0.334IN		
Cr	0.28%	Rebar Deformation Avg. Heigh	0.030IN		
Ni	0.10%	Rebar Deformation Max. Gap	0.120IN		
Mo	0.033%				
V	0.000%				
Cb	0.000%				
Sn	0.012%				
Al	0.002%				
Ti	0.001%				
N	0.0127%				
Yield Strength test 1	69.3ksi				
Yield Strength test 1 (metri	478MPa				
Tensile Strength test 1	106.2ksi				
Tensile Strength 1 (metric)	733MPa				

THIS MATERIAL IS FULLY KILLED, 100% MELTED AND MANUFACTURED IN THE USA, WITH NO WELD REPAIR OR MERCURY CONTAMINATION IN THE PROCESS.

REMARKS :

03/21/2011 01:40:46
Page 1 OF 1

Appendix 2: Additional Concrete Data and Reports

A2.1 Concrete Batch 1 Report

```

*Auburn Univ. - Engineer Dept  HARBERT ENGINEERING DEPT          FORM # A 73192
                                                                    CONTROL # 246819
                                                                    DATE: 10/04/11
                                                                    TIME: 14:49:01

CST:10504872  JOB:112  MIX:AL-AF1C  ALDOT Bridge Sup  PLANT:622
WATER ADJ: -8.0 GAL/CUYD  ADMIX %: 100 100 100  MAX ADD WTR: 48.0

AMT: 6.000 CUYD  DELIVERED: 6.000 CUYD
TRUCK ID:0439  DRIVER ID:3300

BATCH 1 OF 1 CUYD: 6.000
ZEROS:AGGA 5LB CMTA -8LB WTRA -0LB
DESCRIPTION MTRL BIN AMOUNT TARGET SUBSTITUTED_IN_PREVIOUS_MTL_____
#67 Limeston 208 AGA3 11490LB 11514
Conc. Sand 301 AGA2 7715LB 7756
Cement 102 CMA1 H 3066LB 2976
C - Ash 111 CMA2 H 771LB 744
Water 600 WTA1 824LB 828
ADVA 140M 442 ADA4 1440Z 144
Darex II AEA 463 ADA1 90Z 9
Daratard 37 483 ADA3 720Z 72
% MOIST: AGA3 1.0 AGA2 4.0
ZEROS:AGGA 5LB CMTA 14LB WTRA 4LB
TOLERANCES AGG/SND: -0.337% CMT/FLY: 3.155% WTR: -0.474% ADM: 0.000%
ACTUAL WATER/CEMENT RATIO: 0.324
  DRY  AGG  SAND  CMT/FLY  ADM  WATER  TOTAL
WEIGHTS 18795LB 0LB 3816LB 8.58LB 1239LB 23858LB

TEMPER WATER AMT: 0 GAL TIME: 14:53:09
    
```

Note: ADVA 140M was not included in the final mix but was included on the batch report as a standard mix design which includes ADVA 140M was used.

A2.2 Concrete Batch 2 Report

SOLD TO DELIVERED TO
 *Auburn Univ. - Engineer Dept HARBERT ENGINEERING DEPT

FORM # A 73564
 CONTROL # 247190
 DATE: 10/25/11
 TIME: 07:18:06

CST:10504872 JOB:13 MIX:AL-AF1C ALDOT Bridge Sup PLANT:622
 WATER ADJ: -8.0 GAL/CUYD ADMIX %: 100 100 100 MAX ADD WTR: 52.0

AMT: 6.500 CUYD DELIVERED: 6.500 CUYD
 TRUCK ID:3514 DRIVER ID:3518

BATCH 1 OF 1 CUYD: 6.500

ZEROS:AGGA 2LB CMTA 21LB WTRA -1LB

DESCRIPTION MTRL BIN AMOUNT TARGET SUBSTITUTED_IN_PREVIOUS_MTL_____

#67 Limestone 208 AGA3 12493LB 12474

Conc. Sand 301 AGA2 8478LB 8403

Cement 102 CMA1 3248LB 3224

C Ash 111 CMA2 811LB 806

Water 600 WTA1 895LB 897

ADVA 140M 442 ADA4 1560Z 156

not added

Darex II AEA 463 ADA1 90Z 10

Daratard 37 483 ADA3 800Z 78

% MOIST: AGA3 1.0 AGA2 4.0

ZEROS:AGGA 5LB CMTA 1LB WTRA 12LB

TOLERANCES AGG/SND: 0.439% CMT/FLY: 0.729% WTR: -0.198% ADM: 0.513%

ACTUAL WATER/CEMENT RATIO: 0.334

DRY	AGG	SAND	CMT/FLY	ADM	WATER	TOTAL
WEIGHTS	20518LB	0LB	4079LB	9.34LB	1342LB	25949LB

A2.3 Complete Batch 1 Cylinder Test Data

Table A2.3-1: Complete Cylinder Test Data for Concrete Batch 1

Pour Date	Pour Time			
10/4/11	6:45pm			
Cylinder Test Date	Cylinder Test Time	Cylinder Age (days)	Force Reading(lbs)	Cylinder Strength (psi)
10/12/11	1:15pm	7	61780	4920
10/12/11	1:15pm	7	58220	4630
10/12/11	1:15pm	7	56370	4480
10/18/11	3:11pm	14	62570	4980
10/18/11	3:11pm	14	65260	5190
10/18/11	3:11pm	14	66960	5330
11/1/11	1:15pm	28	68200	5430
11/1/11	1:15pm	28	66480	5290
11/1/11	1:15pm	28	66390	5280
1/4/12	3:15pm	92	66010	5250
1/4/12	3:15pm	92	66550	5290
1/4/12	3:15pm	92	65710	5230
4/11/12	12:15pm	190	64900	5160
4/11/12	12:15pm	190	62260	4950
4/11/12	12:15pm	190	59440	4730
5/10/12	3:00pm	219	57850	4600
5/10/12	3:00pm	219	56720	4510
5/10/12	3:00pm	219	60280	4800

A2.4 Complete Batch 2 Cylinder Test Data

Table A2.4-1: Complete Cylinder Test Data for Concrete Batch 2

Pour Date	Pour Time			
Cylinder Test Date	Cylinder Test Time	Cylinder Age (days)	Force Reading (lbs)	Cylinder Strength (psi)
10/25/11	11:45am			
11/1/11	1:15pm	7	56290	4480
11/1/11	1:15pm	7	53250	4240
11/1/11	1:15pm	7	55240	4400
11/8/11	3:11pm	14	63380	5040
11/8/11	3:11pm	14	64260	5110
11/8/11	3:11pm	14	62450	4970
11/22/11	2pm	28	66980	5330
11/22/11	2pm	28	65040	5180
11/22/11	2pm	28	64660	5140
1/23/12	4:03pm	90	54330	4320
1/23/12	4:03pm	90	63780	5070
1/23/12	4:03pm	90	65650	5220
8/6/12	9:46am	286	61340	4880
8/6/12	9:46am	286	58230	4630
8/6/12	9:46am	286	61590	4900
9/16/12	5:12pm	327	50850	4050
9/16/12	5:12pm	327	65490	5210
9/16/12	5:12pm	327	65050	5180